USDOT Tier 1
University Transportation Center
on Improving Rail Transportation
Infrastructure Sustainability and Durability

Final Report VT-2

DETECTING FOULED BALLAST USING FORWARD-LOOKING INFRARED RADIOMETER (FLIR) TECHNOLOGY

By

Dr. Mehdi Ahmadian, J. Bernard Jones Chair Professor
Director & Founder of CVeSS and RTL
Department of Mechanical Engineering
ahmadian@vt.edu

Yongwen Tan, Visiting Scholar
Department of Mechanical Engineering
yongwen@vt.edu

Sayed Mohammad Hosseini, Graduate Research Assistant
Department of Mechanical Engineering
mohammadhosseini@vt.edu

August 10, 2020

Grant Number: 69A3551747132

DISCLAIMER

ABSTRACT

The feasibility and limitations of Forward Looking Infrared Radiometer (FLIR) Aerial Technology for detecting fouled ballasts is studied in this project. The method is intended to provide an efficient and ready-to-use approach that can help the railroads detect fouled ballasts in their early stages. Ballast fouling commonly occurs as a result of fine particles clogging off water passage through them. Subsequently, this results in trapped water that often results in poor foundation strength, rotting of the ties, and other ill effects.

This study includes a novel approach to evaluate the railway ballast fouling by using thermal imaging techniques. A simple setup for implementing ballast fouling of different amounts have been implemented in the lab. For the purpose of laboratory testing, the camera is set up in stationary and moving configurations. The thermal characteristics of clean and fouled ballasts are studied using FLIR cameras that can be used onboard rolling stock, Hyrail trucks, or drones. Laboratory tests are primarily performed to measure the surface temperature changing rate of clean and fouled ballasts in response to ambient temperature changes.

The test results indicate that clean and fouled ballasts have different thermal characteristics. In particular, different thermal patterns are obtained during naturally-occurring daily temperature change. The test results also indicate that the FLIR cameras can be used on a moving platform for quick scanning of thermal images of the ballasts that could be used for assessing the early stage of fouling.

Keywords: Forward looking infrared radiometer, ballast, ballast fouling, thermal image technique

TABLE OF CONTENTS

LIST OF FIGURES

LIST OF TABLES

EXECUTIVE SUMMARY

Railway Technologies Lab, with the application of FLIR camera, performed a series of tests on the temperature changes of railway ballast in response to naturally-occurring ambient changes. The tests indicate that the surface temperature is detectable and is influenced by the ballast fouling condition.

Laboratory tests are further conducted for detecting temperature variations in both stationary and moving configurations. The results show the feasibility of FLIR technology for the intended research purpose.

Thermocouples are further used for the purpose of measuring the temperature changes below the surface. The results validate the effectiveness of the application of the FLIR camera and show a temperature difference under various conditions.

A numerical heat transfer model is built for railway ballast, and an indoor experiment is conducted for validating the effectiveness of the proposed model. The simulated results agree with the experimental results.

An extensive amount of simulations is performed based on the numerical model. They show different thermal behaviors for the ballast under various fouling conditions. The simulations give the range of the temperature difference between the ballast samples under various fouling conditions.

INTRODUCTION

This project examines the feasibility and limitations of Forward-Looking Infrared Radiometer (FLIR) Aerial Technology for detecting fouled ballast. The method is intended to provide an efficient and ready-to-use approach that can help the railroads detect fouled ballast in their early stages for using FLIR onboard rolling stock, Hyrail trucks, or drones. This study includes a novel approach to evaluating the railway ballast fouling by using thermal imaging techniques. Both laboratory experiments and numerical simulations are performed based on the thermal characteristics of clean and fouled ballast. Laboratory tests are primarily performed to measure the surface temperature changing rate of clean and fouled ballast in response to ambient temperature changes under both stationary and moving configurations. The test results indicate that the FLIR cameras can be used on a moving platform for quick scanning of thermal images of the ballast that could be used for assessing the early stage of fouling. A numerical model of ballast heat transfer is built and analyzed with numerical simulations under various ambient conditions. The results show that there exists different thermal behavior between clean and fouled ballast in various conditions, which proves the effectiveness of the proposed FLIR based detection approach.

Background

Ballast, commonly used on railway tracks, plays an essential role in maintaining track stability and operating requirements (Lim 2004). The critical functions of the ballast include supporting periodic rail loading, preventing track deformation, and accommodating water drainage from its surface to the foundation (Indraratna and Salim 2005, Janardhanam, and Desai 1983,and Indraratn, et al. 2011). The aggregate formation of the track efficiently accommodates water drainage, unless it is clogged up with fine particles that impede drainages. Such fine particles can be introduced as blow away of dry bulk material that is carried on the rail such as coal, soybean, etc. or the breakup of the ballast itself. The latter can result due to aging, tamping, or both (Anbazhagan, et al. 2012 and Bruzek et al. 2016)

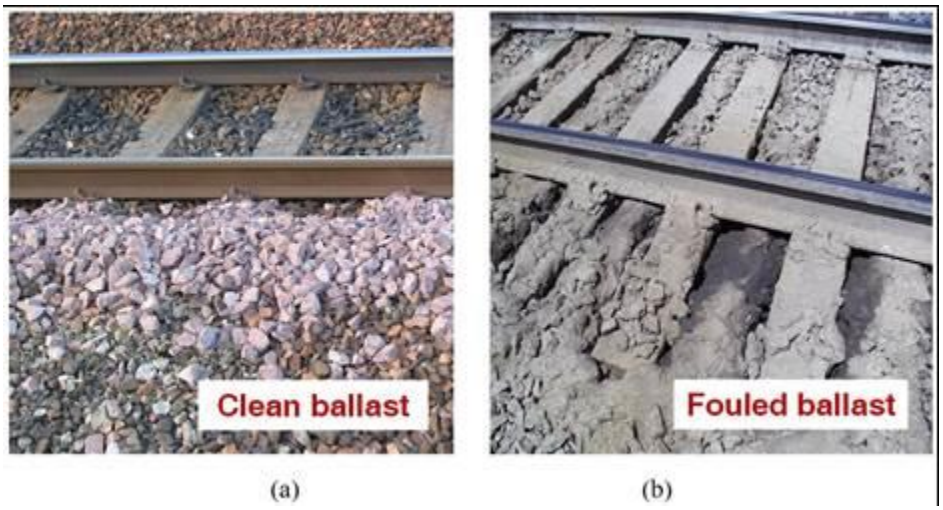

Figure 1 (a) clean ballast and (b) fouled ballast on railroad

When mixed with other materials, the ballast is considered to be “fouled.” Over time, the water drainage restriction caused by fouled ballast results in water retention within the ballast, which

eventually forms a slurry that gets pumped to the surface, as a result of vibrations caused by the rolling stock. Such an occurrence, which is shown in Figure 1b next to the clean ballast on a railway track, is commonly referred to as "clay pumping". The clay pumping causes an increase in water retention and water pressure that eventually leads to the decreased overall strength of the ballast layer (Indraratna et al. 2013) . Early detection of fouled ballast is quite critical for mitigating any problems before they progress to problems that require costly ballast/tie changes, or poor track stability.

There currently exist some technologies for the detection of fouled ballast. The traditional approach is to dig trail pits at regular intervals along the track (Jack and Jackson, 1999, Brough et al. 2003, and Xu and Zhang, 2010). Although this provides an accurate examination of the ballast' fouling condition through the trail pits, it is time-consuming, condition-driven, and limited to the location of the trail hole (Leng et al. 2010 and Al-Qadi et al. 2010). In recent years, ground-penetrating radars (GPR) have received increased attention as an invasive method of assessing track foundation conditions (Shao et al. 2011, Clark et al. 2001, and Silvast et al. 2010). GPR detects the wave reflected from the ballast, making it possible to calculate the thickness of each ballast layer by measuring the time of flight for radar waves (Hugenschmidt 2000). Compared with the traditional approaches, GPR is a non-destructive method capable of providing continuous information regarding the location and thickness of the fouled ballast. The practical application of GPR, however, is limited since it requires fairly complex equipment, slow, and interrupts traffic flow.

Objectives

This project aims to provide a novel technology for detecting the railroad ballast fouling at its early stages.

Overall Approach

Addressed on the difficulties for early-stage detection of ballast fouling, the methodology of this project includes four major parts, which are the calibration of the camera, application of the camera, and numerical studies. Firstly, the FLIR camera that is applied for our purpose, is calibrated by analyzing the influence of height, surface material, distance, light, self-temperature, and frequency of taking pictures. Temperature reading and image quality from those tests are compared and discussed.

Secondly, in order to further explore the capability of the FLIR camera for detecting the ballast fouling condition, the camera was used to detect the surface temperature difference between the clean ballast, partially fouled ballast and fully fouled ballast. The tests are performed in both stationary conditions and moving configurations. For stationary configuration, tests are performed both indoors and outdoors where the camera is fixed by an 80/20 structure that is able to adjust the height. For the moving configuration, tests are only conducted outdoors with the camera mounting on the back of a truck, which is moving at a speed ranging from 5 mph to 25 mph during the test. Among those tests, clean and fouled ballast are considered for the purpose of comparison. The camera is taking pictures at a frequency of one picture per second, which is the highest frequency the camera can perform. Temperature reading and image quality from those tests are mainly discussed.

Thirdly, to further understand the thermal behavior of ballast, a series of tests are performed with the application of thermocouples for their convenience of accurate and direct measurement. In total, 32 thermocouples are placed at the top surface, 2-inch, 4-inch, 8-inch and 12-inch deep of ballast. In those tests, clean, fully fouled and partially fouled ballast are placed side to side when exposing to naturally-occurring ambient temperature changes. Tests are designed to compare the thermal behavior of ballast at both dry and wet conditions. The first round of experiments is conducted to analyze the temperature of the ballast at the dry condition. Then water is added into all ballast, where the ballast with more fouling has more water content, and the experiment is performed again. Notably, tests are performed in two kinds of containers to simulate the condition of water draining through away and the condition that water is trapped inside the ballast.

Lastly, we build a one-dimensional conductive heat transfer model for studying the thermal behavior of ballast. The radiant boundary condition is considered for the upper boundary to simulate the naturally-occurring temperature change. And the lower boundary is assumed to be at a constant temperature. The model is validated by an indoor experiment for both clean and fouled ballast. A series of simulation studies are carried out to study the effect of fouling content and water content on the thermal ballast of ballast. The model provides the convenience of analyzing the temperature data at all depth and all ballast conditions. Then the simulation result is further compared to the real data acquired by the FLIR camera.

Scope

The work presented here includes the initial study of the application of the FLIR camera, where laboratory experiments and numerical studies are carried out for this purpose. For the sake of initial studies, the effort made in this project does not include any on-site experiment and measurement. The contribution of this present work could be summarized as a guide to further studies.

Organization of the Report

The remainder of this report is as follows. In section 2 we present the laboratory experiments based on the FLIR camera. In section 3 we discuss the numerical model and the simulation studies. And in section 4 we present the conclusion and discussion.

APPLICATION OF FLIR CAMERA FOR BALLAST FOULING DETECTION

Technical background

The FLIR aerial technology is often referred to as the unmanned aerial vehicle (UAV) based FLIR camera technology. UAV enables the FLIR camera to take quick temperature measurements over large areas. Figure 2 illustrates the schematic of how the FLIR camera measures the surface temperature of an object. The measured object emits electromagnetic radiation in the infrared region of the electromagnetic spectrum if its temperature is above 0 K (i.e. -273°C) (Bagavathiappan, et al. 2013). An infrared detector is employed in the FLIR camera to detect the infrared energy emitted by the object. The infrared energy (q) is then applied to calculate the surface temperature of the object (T) by the law of Stefan-Boltzmann (Arpaci and Arpaci 1966) :

$$q = A\varepsilon\sigma T^4 \quad (1)$$

where A is the area of the emitting surface, ε is the emissivity of the emitting surface, σ is the Stefan-Boltzmann constant, and T is the absolute temperature of the object.

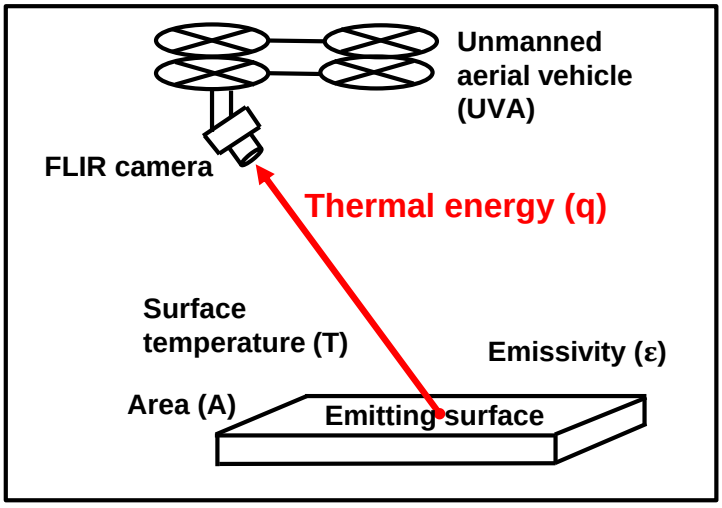

Figure 2 Schematic setup and theory of the FLIR aerial technology

The FLIR aerial camera is a newly-developed technology that has recently drawn strong attention. There are many novel applications of thermal cameras in some recent studies. For instance, Gallardo et al. (2018] reviewed and investigated the key characteristics of commercial sensors and platforms related to FLIR cameras and UVA systems. The possibility of applying FLIR aerial technology on inspection of photovoltaic plants is demonstrated in their study. As shown in Figure 3, the faulty modules are obvious in the thermal image because of its higher temperature.

Burud et al. (2018) investigated the possibilities of the adoption of the FLIR aerial technology in the urban surface study. Their results confirmed that this technology provides information about temperature distribution on a large scale. Ariwoola and Raheem (2016) applied the FLIR aerial technology to detect the energy loss of buildings, as shown in figure 4. The flexibility of the FLIR aerial technology provides a significant convenience in measuring the surrounding and top

surfaces of buildings. FLIR aerial technology is also applied for early sinkhole detection (Lee et al. 2016), volcanic environment monitoring (Amici et al. 2013) and bridge crack detection (Omar and Nehdi 2017). Those researches demonstrated the advantage of FLIR aerial technology for remote sensing, data visualization, and easy instrumentation.

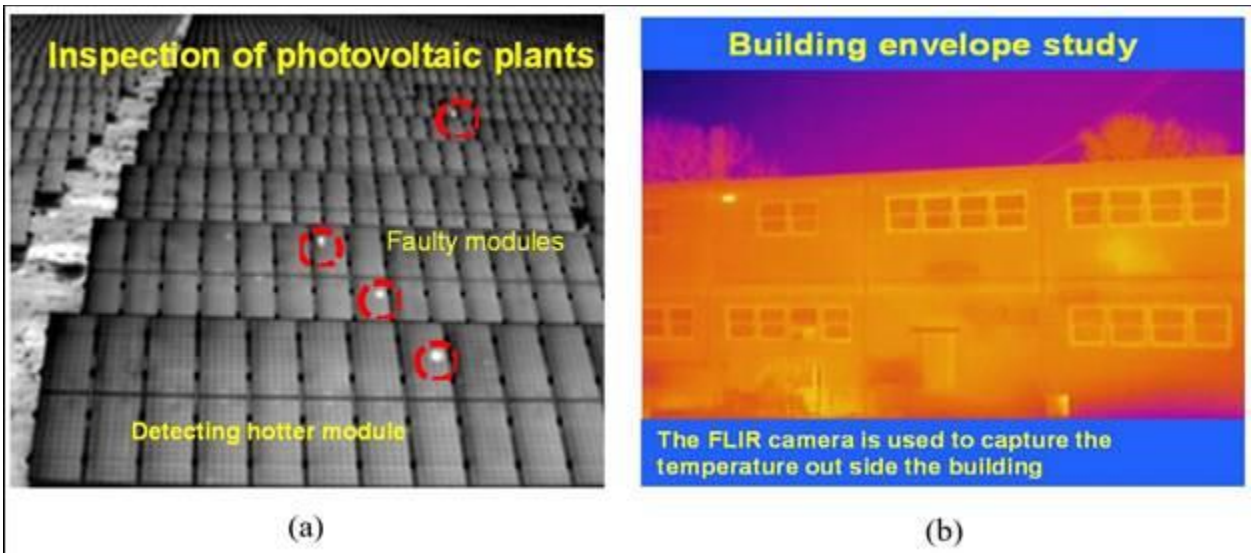

Figure 3 Application of FLIR VUE PRO R camera for research purposes: (a) Detecting the faulty modules in the photovoltaic plant. (b) Calculating the building envelope

In this project, we chose FLIR VUE PRO R because it is potentially designed for drones, which ensures the low weight and high vibration resistance. The accuracy of this camera is not as precise as other scientific cameras, but it is good enough for our initial study of the application of this technology. The best thing about this camera is that it is blue-tooth controlled, and you can change setting in the app called "FLIR UAS". Those setting includes the emissivity of the object, the humidity, the distance.

Figure 4 FLIR VUE PRO R (a) side view; (b) top view

The field view of the camera is 45°, which is wide enough, and the IR resolution is high, with 336*256 pixels in each picture. The operating temperature allows the camera to be used in summer and winter days without damaging the inner modules. Also, the frequency of the camera is as high as 30 Hz, which means in the video mode, 30 pictures are taken in each second, which ensures the quality of the video. However, if operating the camera in video mode, the thermal video will only include the relative radiation, meaning that it will show the relatively higher temperature and relatively low temperature in different colors, but it cannot directly provide temperature readings. In our research, the camera is mainly used to take thermal pictures. Notably, the accuracy of the camera is ± 5% or 5 ℃. According to the FLIR company, the drone-based camera is able to provide accurate temperature reading in a stationary configuration. But when the camera is mounted on a drone, the temperature reading will be greatly influenced by the ambient environment like wind, solar radiation, vibration, and humidity. So, when using this camera in a moving configuration, all those influence factors have to be considered.

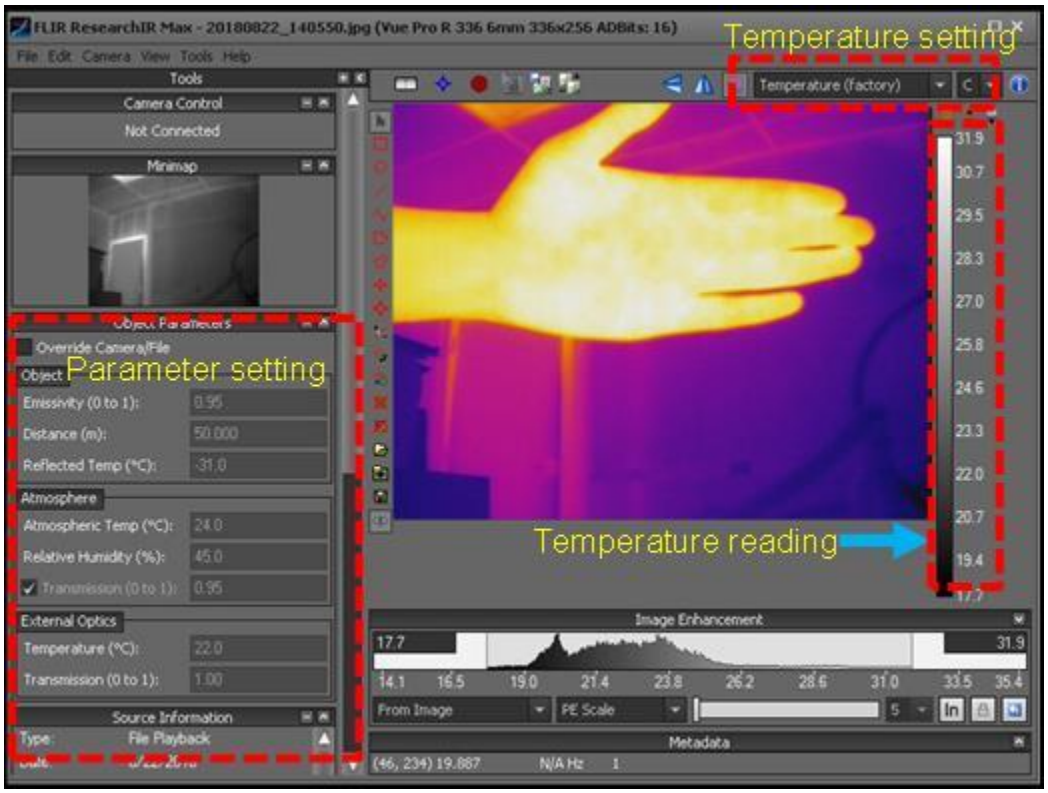

Figure 5 Research IR provided by FLIR company

FLIR camera calibration

Test 1: The influence of camera self-heating up

The internal modules of the FLIR camera will heat up by the time of use. To analyze the influence of the camera's temperature on the temperature reading, an indoor test is conducted, and the test setup is shown in Figure 6. The wood plate is covered with black electric tape, which is generally considered to have the emissivity of 0.95. The camera is facing at the wood plate at a vertical

angle, and the distance is 30 cm. A thermocouple is placed on the top surface of the camera to measure the temperature of the camera. Another thermocouple is placed on the surface of the wood plate to compare the temperature measurement from the FLIR camera. A thermometer is used to measure the ambient temperature. Before the test start, the wood plate is allowed to reach a thermal equivalent with the ambient.

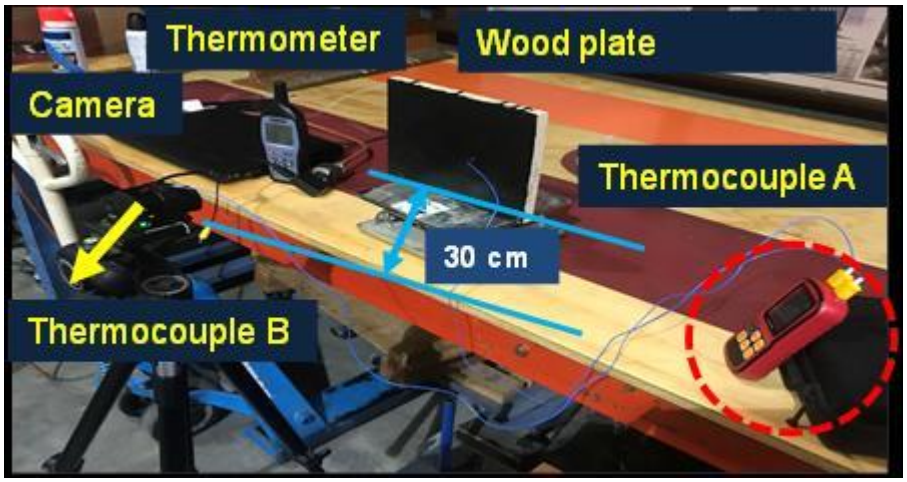

Figure 6 Experiment setup for measuring the influence of temperature

Figure 7 shows the temperature of the wood plate measured by both the FLIR camera and thermocouple. And, it shows the temperature of the camera itself. The test duration time is 30 minutes, and it could be observed that the temperature of the camera is rising quickly from 90 to 110 °F. The temperature reading from the thermal camera is close to that of thermocouples at the beginning of the test. But the difference increases as the camera is heating up. It could be concluded that when the camera is heating up, the measured object will seem to be hotter. This indicates that the use of the camera should not exceed 20 minutes to achieve higher accuracy.

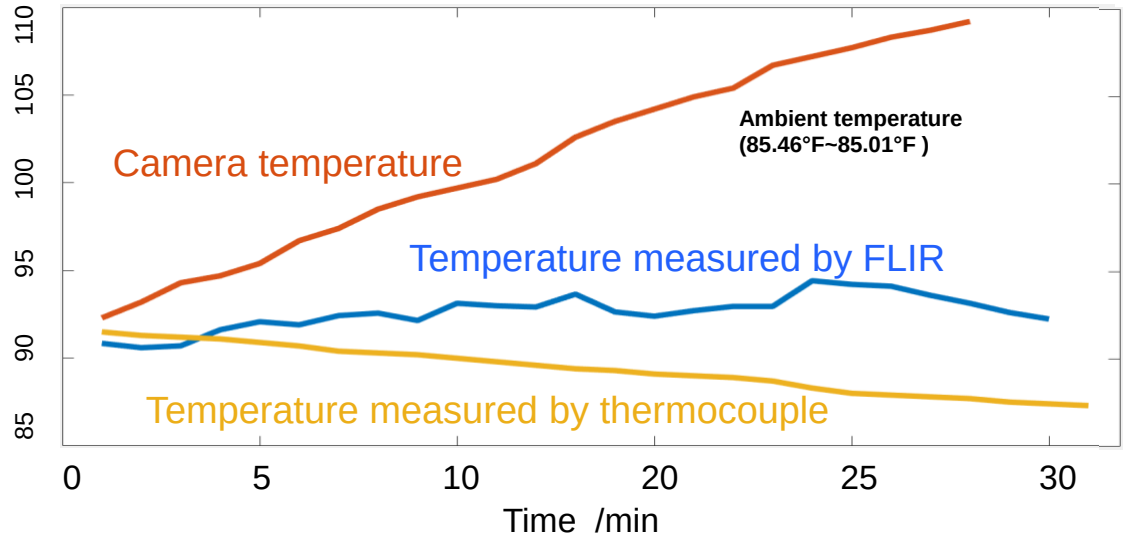

Figure 7 The temperature result measured by FLIR camera and thermocouple

Test 2: The influence of the vignetting effect of the camera

Also, the vignetting of the camera is also analyzed using the same experimental setup shown in Figure 8. The camera is set to take 140 images in 15 mins, and the thermal picture is divided into three sections: the central section A, which occupies 50% of the image; a larger section B, which occupies 75% percent of the images; and section C which is the whole image. The average temperature in the specified area is calculated for all 140 thermal images. The result is shown in Figure 9, and it could be observed that the mean temperature of section A is higher than section B and C. It is because that there is less optical power absorbed by the edge of the lens, which makes the edge of the thermal image seems to be cooler. It indicates that the measured object should be placed on the central part of the camera to ensure higher accuracy.

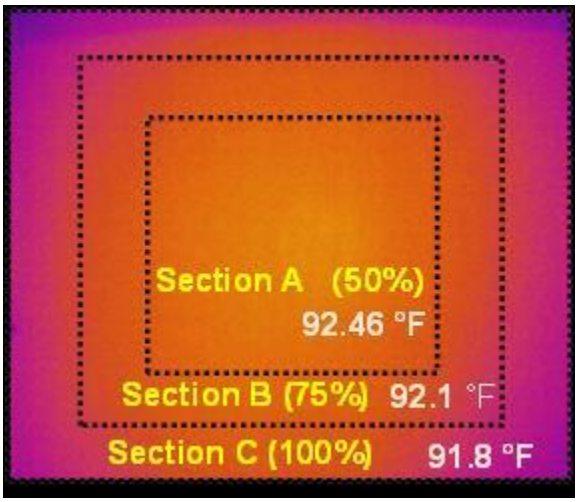

Figure 8 The average temperature of the thermal picture at three sections

Test 3: The influence of ambient light on the temperature measurements

The effect of ambient light is analyzed using the same experiment set up shown in figure 9. The FLIR camera is used to capture the temperature of the wood plate while the ceiling light is turned on and turned off. 30 pictures are taken in a row to compare the performance of the camera with and without ambient light. The result is shown in Figure 10. It is obvious that the temperature reading of the wood plate is not influenced by the ambient light.

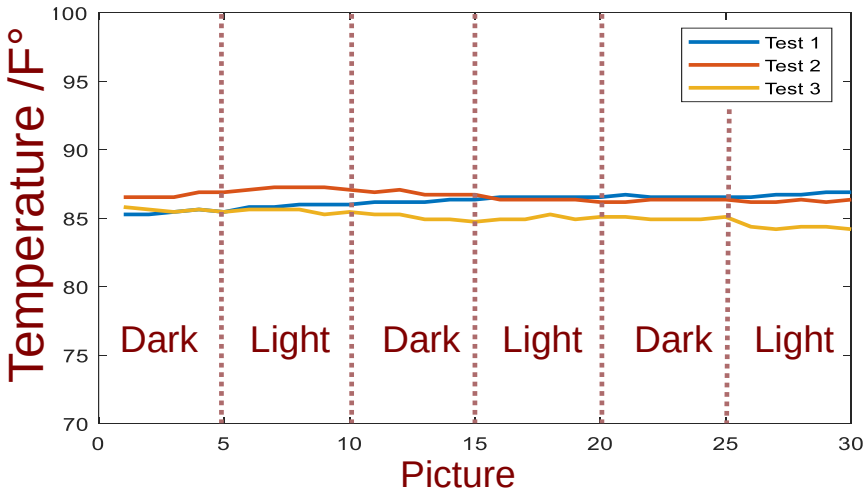

Figure 9 The thermal result with and without ambient light

Test 4: The influence of PPM on camera's performance

The PPM is defined as the number of pictures taken per minute. In order to analyze the influence of PPM on the performance of the FLIR camera, four PPM (0.2, 1, 10, 60) are applied in the test. Before the test starts, the wood plate is allowed to reach thermal equivalent with the ambient. The test duration is 60 minutes and the result is shown in Figure 10. The result shows that the temperature reading is not directly influenced by the PPM.

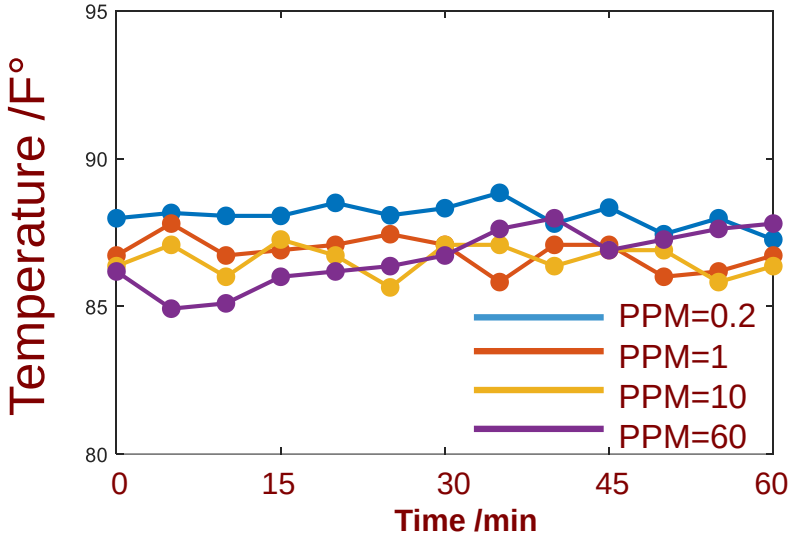

Figure 10 The thermal result with different PPM

Application of FLIR Camera for Detecting Ballast Fouling Condition

Laboratory Tests in a Stationary Configuration

Laboratory tests in a stationary configuration are conducted to determine whether the FLIR camera can detect the temperature difference. The temperature changes of the ballast with various fouling conditions are tested and compared with that of clean ballast. Among these tests, the clean and fouled ballast samples are exposed to naturally-occurring ambient temperature changes.

A stationary structure is built up by 80/20 beams to fix the FLIR camera. The camera is set at 2.4 meters above the ground and 60 degrees from the horizontal direction to minimize the sun glints. All test samples are exposed to the ambient environment. Two tests (test A and test B) are performed to provide validation for the simulation results, in particular, to investigate the temperature difference between clean and fouled ballast. Test A focuses on the comparison of the dry-soil-fouled ballast and wet-soil-fouled ballast, whereas Test B is related to the fouled ballast with standing water.

Test A The setup for test A is shown in Figure 11. Test samples are taken from four types of ballast including clean, moist, dry-soil-fouled, and wet-soil-fouled ballast, which are shown in Figure 12. The testing samples are placed in four hand-made shallow wooden boxes. Each sample contains the same amount of ballast (22.7 kg). The dry-soil-fouled and wet-soil-fouled ballast are made by mixing with an additional 11.3-kg of soil, at a fouling ratio of 50%. It is worth noting that both samples of moist and wet-soil-fouled ballast do not involve any standing water. Test A was performed from 4:00 pm (ambient temperature = 60 °F) to 6:25 pm (ambient temperature = 54 °F).

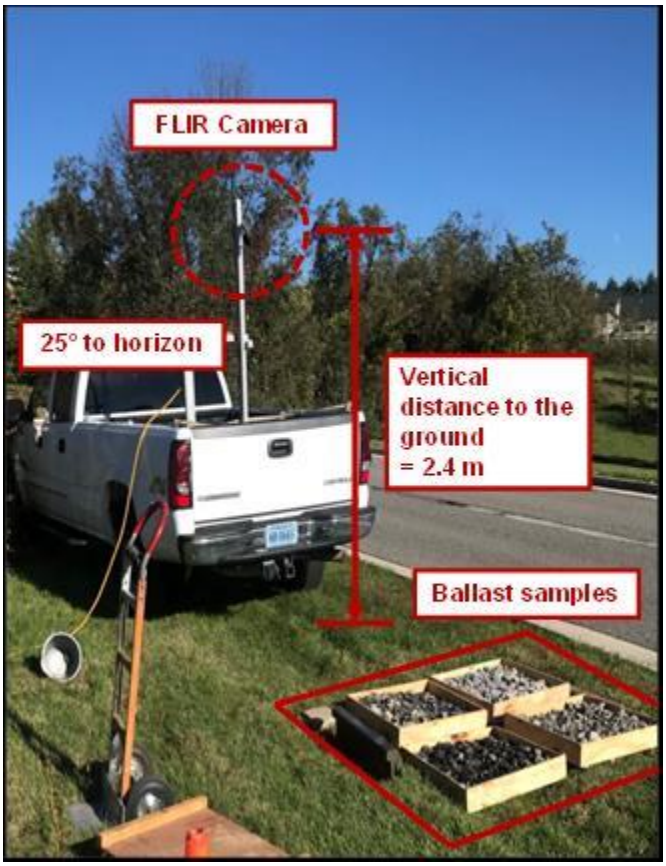

Figure 11 Setup for test A

Figure 12 Ballast samples used in test A

Test B In test B, fouled ballast with standing water are taken into consideration, including dry-soil-fouled ballast (25% fouled), dry-soil-fouled ballast (50% fouled), wet-soil-fouled ballast, and wet-soil-fouled ballast with standing water. In contrast, to test A, the ballast samples are placed in deeper containers, as shown in Figure 13. The 80/20 structure used in test A is also applied to this test. Ballast samples are exposed to ambient temperature changes from 2:00 pm (ambient temperature = 64 °F) to 7:30 pm, (ambient temperature = 51 °F).

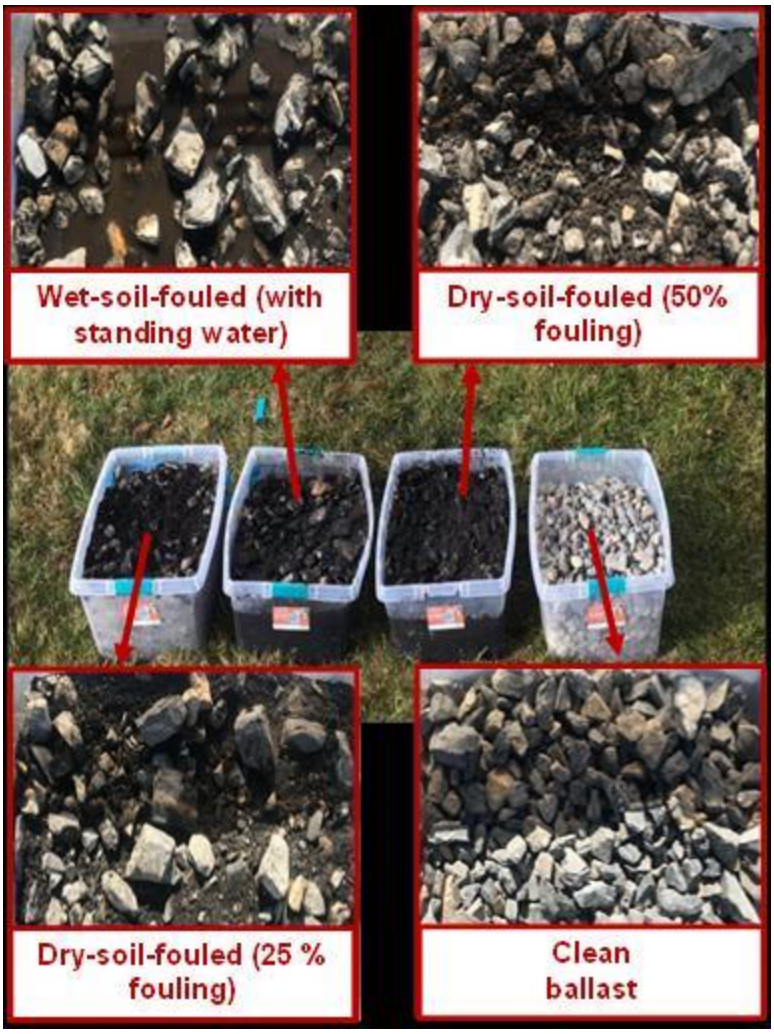

Figure 13. Ballast samples used in test B

Testing Results Discussion

An example of the infrared image taken by the FLIR camera is shown in Figure 14, where different colors represent different temperatures. The Research IR software is used to obtain temperature readings stored in each pixel of the infrared image. The color bar on the right shows the temperature distribution in the image (the unit is °F). The average temperature of the selected area, which is selected to reasonably represent the entire surface of the ballast sample, is calculated using MATLAB. The results of the average temperature of each ballast sample for tests A and B are shown and discussed in the following.

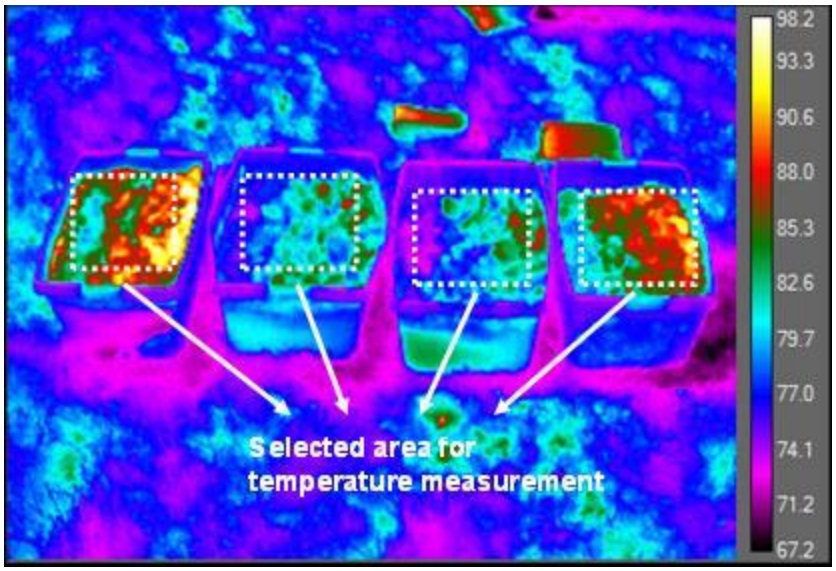

Figure 14. Infrared image of ballast samples in test B

Results of Test A The surface temperatures of the four ballast samples are shown in Figure 15. The temperature of the ballast fluctuates due to periodical auto-calibration of the FLIR camera and external factors such as reflection of sunlight, wind, etc. It is difficult to gather useful information from the raw data. However, the relative temperature is not affected by the camera's auto-calibration, as indicated by the results of the temperature difference in Figure 16.

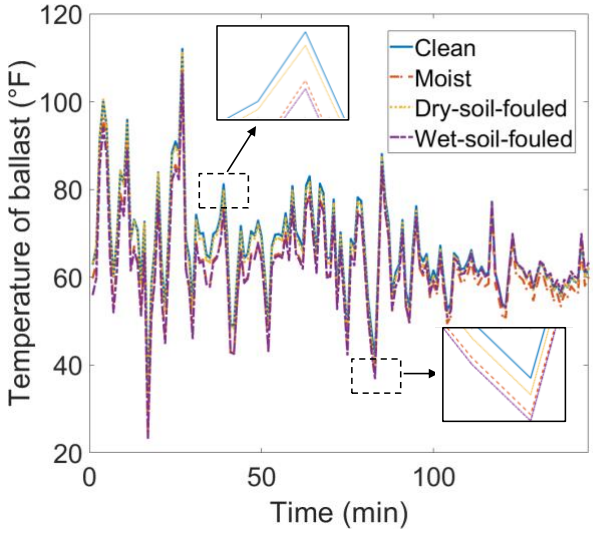

Figure 15 The temperature of clean and fouled ballast (test starts at 10 am)

Figure 16 shows the testing results of the temperature difference between the clean and fouled ballast. Wet-soil-fouled and moist ballast samples are much cooler than clean ballast at the beginning of the test, and then they tend to converge. The main reason for this result is that the heat capacity of moist ballast is much higher than that of dry ballast and soil, which means that moist ballast stays cooler since they require more energy to heat up. The other reason is that the

moist ballast keeps vaporing during this test due to the intense solar radiation. Moreover, no obvious temperature difference is observed between dry-soil-fouled ballast and clean ballast. It is speculated that the conductive heat transfer is limited by the shallow layers of the ballast, which results in a similar thermal behavior between the clean and dry-soil-fouled ballast. A preliminary conclusion can be drawn that there is a temperature difference between the clean and fouled ballast.

Results of Test B The surface temperature difference between the fouled ballast and the clean ballast samples is shown in Figure 16. The results from the wet-soil-fouled ballast (with standing water) show a similar pattern as those of wet-soil-fouled ballast (without standing water) in test A. They are much cooler than clean ballast at the beginning, and the temperature difference decreases over time. Finally, their temperature becomes higher than that of clean ballast, since the wet-soil-fouled ballast needs more thermal energy to heat up. In the case of the dry-soil-fouled ballast, they experience a drop in temperature difference compared to clean ballast, mainly due to the clean ballast heating up faster.

Figure 17 shows the temperature difference resulting from different amounts of fouling. The results for 25% and 50% fouling by weight indicate that there is an inverse correlation between % fouling and a rise in temperature. The wet ballast with standing water behaves significantly different than the other two cases without any standing water. The standing water results in temperatures starting significantly below clean ballast and rising far higher in time. This is mainly due to the difference in the cooling and heating rate of water and the ballast material.

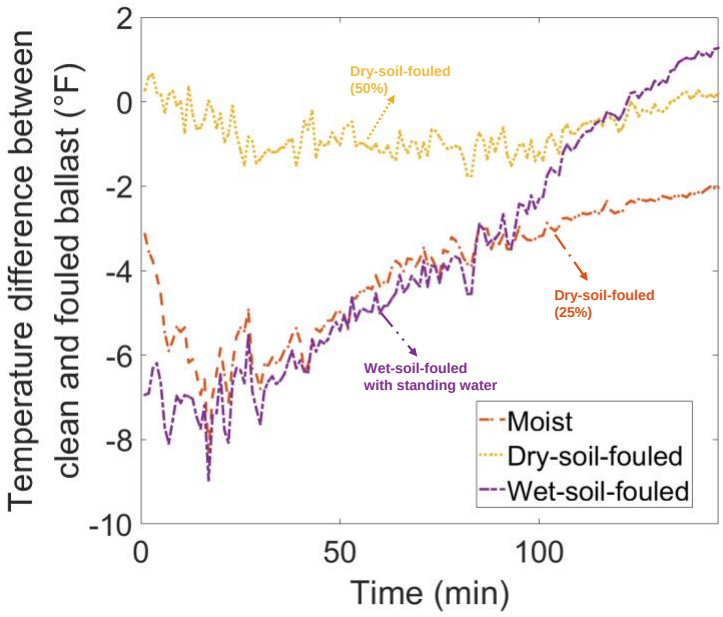

Figure 16. The temperature of fouled ballast compared with clean ballast (test starts at 10 am)

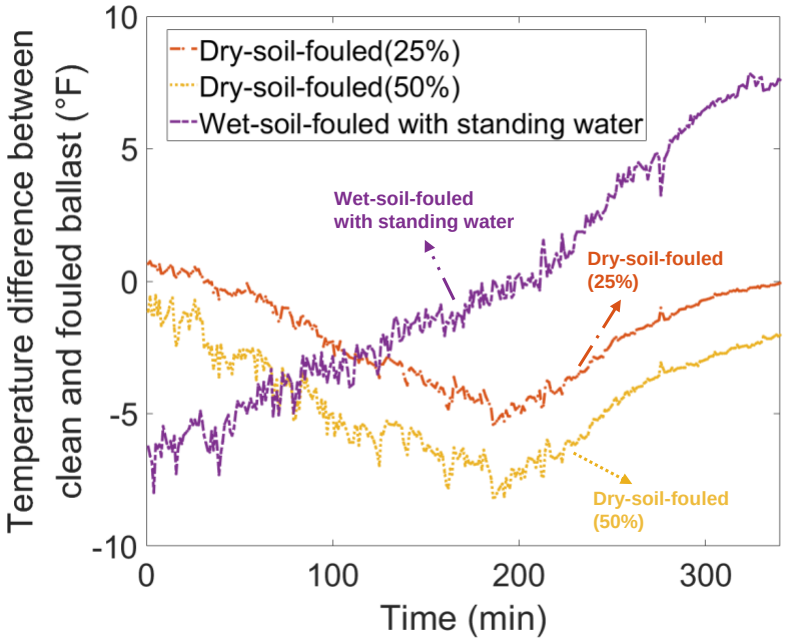

Figure 17 The temperature of fouled ballast compared with clean ballast (test starts at 10 am)

Laboratory Tests in Moving Configuration

This section aims to test the ability of the FLIR camera to detect temperature differences in a moving configuration. The temperature of the fouled ballast is measured by the FLIR camera mounted on a device that moves at various speeds. The test samples are taken from clean and dry soil-fouled ballast (50% fouling). The fouled ballast consists of 11.3-kg soil and 22.7-kg clean ballast. The shallow wooden boxes are used to hold the samples. Notably, each sample contains the same amount of clean ballast. The FLIR camera is mounted on a structure built by 80/20 beams, as shown in Figure 18. The arrangement allows the camera to move along the indoor railway track. The camera is set up at 1.7 m above the sleeper and 60 degrees from the horizontal direction. In the tests, the camera moves at three speeds (0.2, 0.5 and 1 m/s). Tests are performed in six different orders to minimize the influence of the FLIR camera's auto recalibration, as shown in Figure 19.

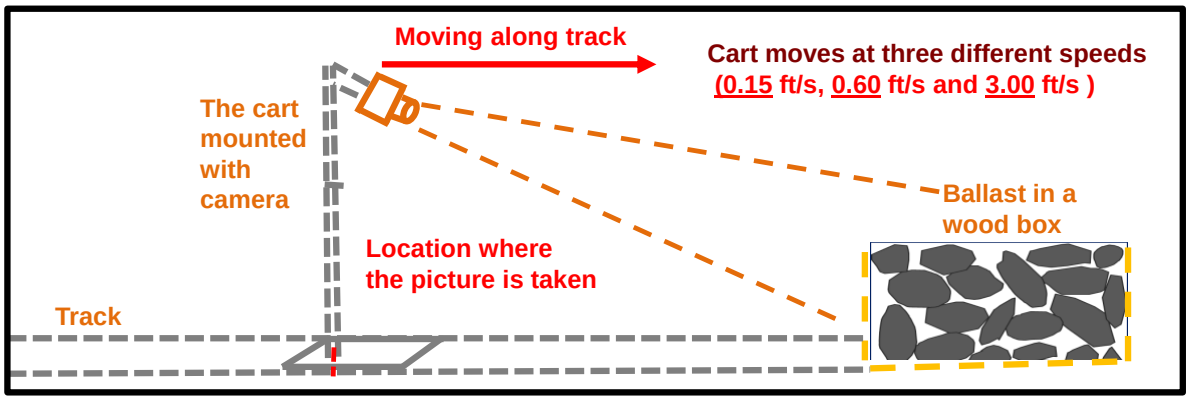

Figure 18. Schematic of the test setup and workflow

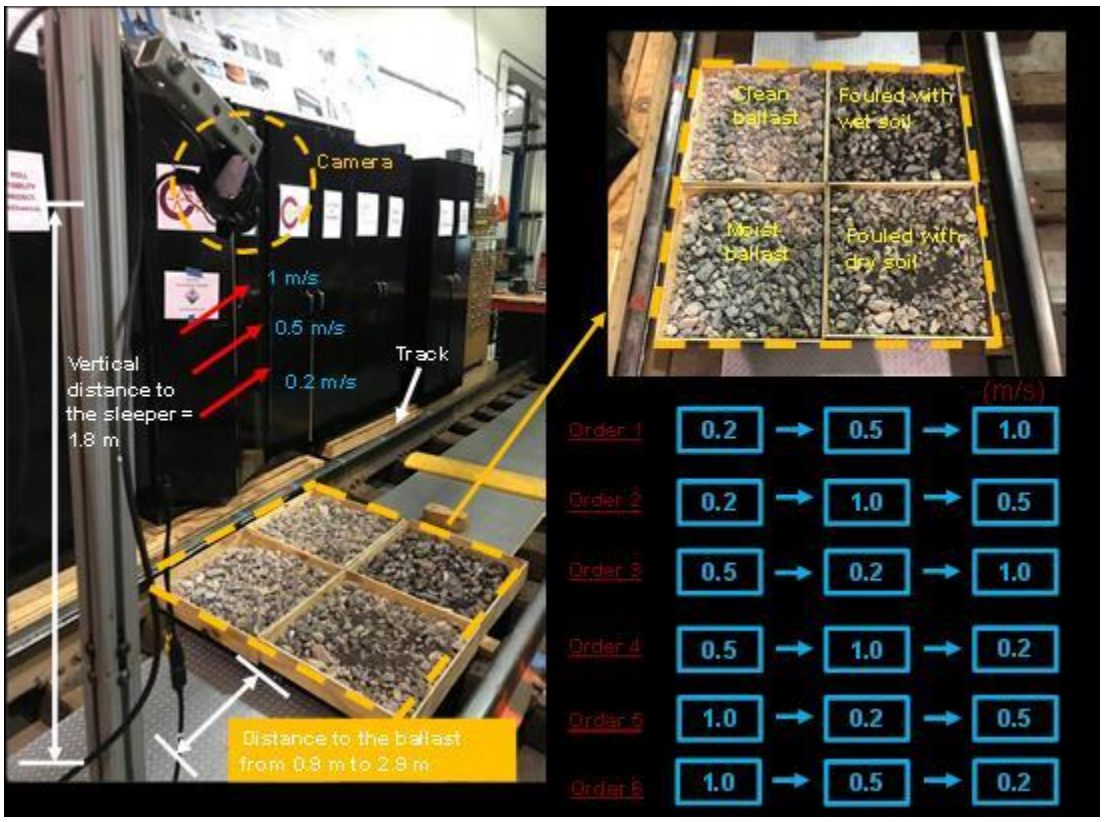

Figure 19 Test setup and test orders

During the test, the ambient temperature changes in a small rage from 75.8 °F to 76.0 °F. Figure 20 shows the infrared image captured by the FLIR camera moving at 1 m/s. The image has good quality and differentiates the temperature difference by colors.

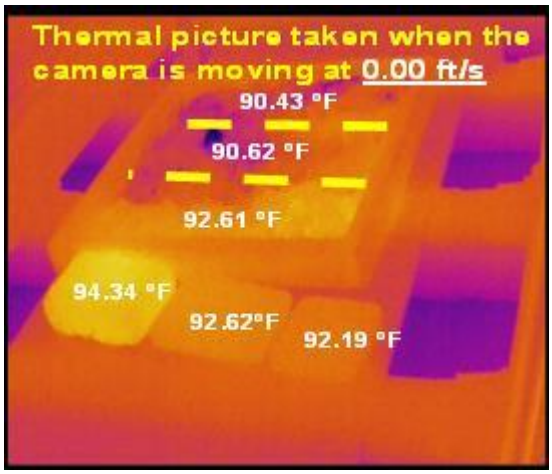

(a)

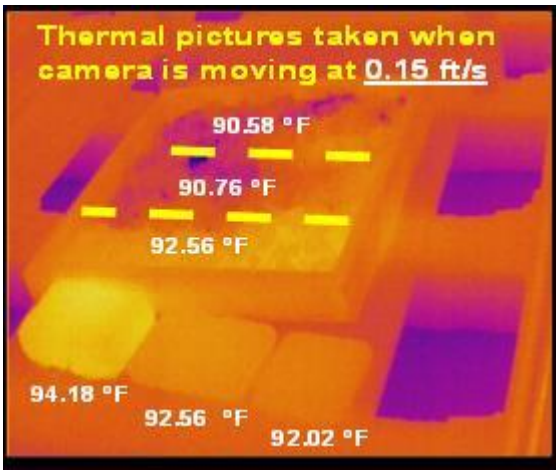

(b)

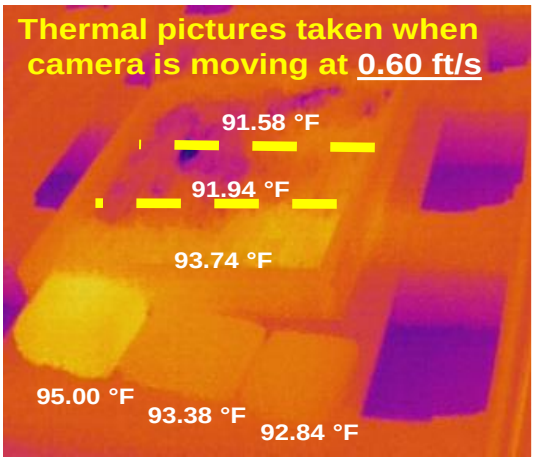

(c)

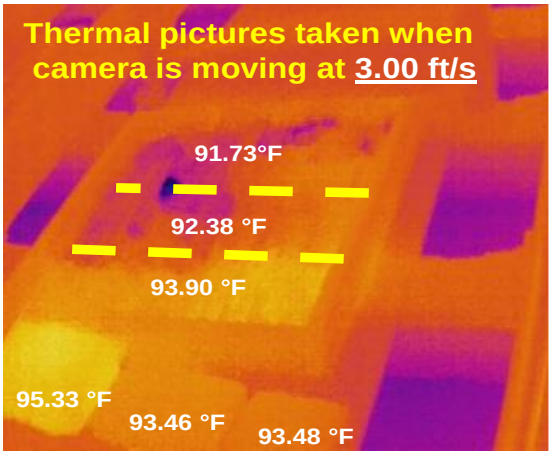

(d)

Figure 20 Infrared image taken by the FLIR camera mounted at 4.41 ft above sleeper

Figures 21 and 22 show the temperature difference between clean and fouled ballast in 6 different orders (speed combinations). There exist temperature differences between the clean and fouled ballast. More importantly, the moving speed does not indicate an obvious influence on the temperature difference readings. It's concluded that the FLIR camera, in a moving configuration, is capable of detecting temperature differences of clean and fouled ballast, and providing stable measurements of temperature difference, which is nearly independent of the moving speed.

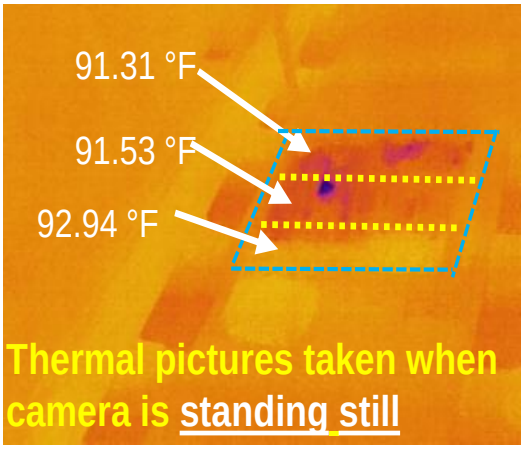

(a)

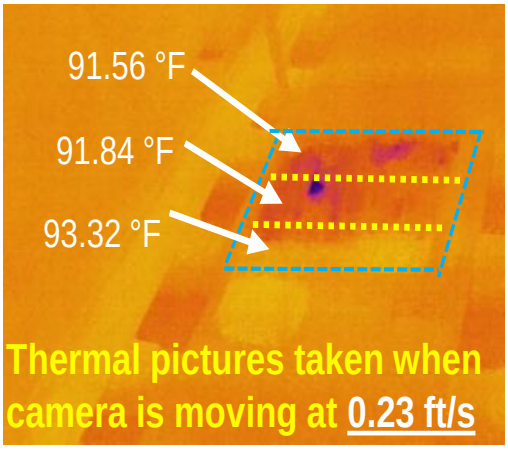

(b)

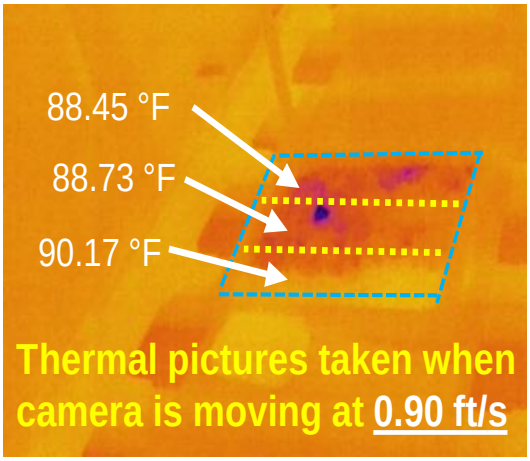

(c)

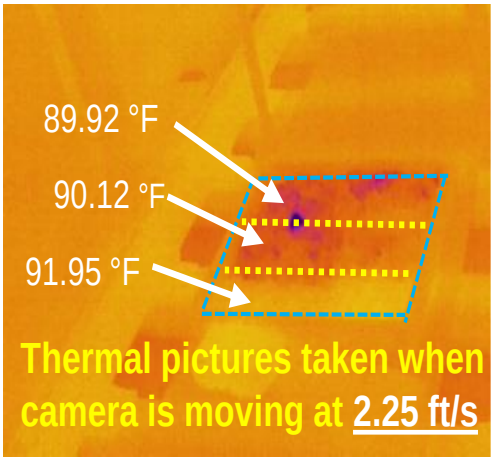

(d)

Figure 21 Infrared image taken by the FLIR camera mounted at 5.83 ft above sleeper

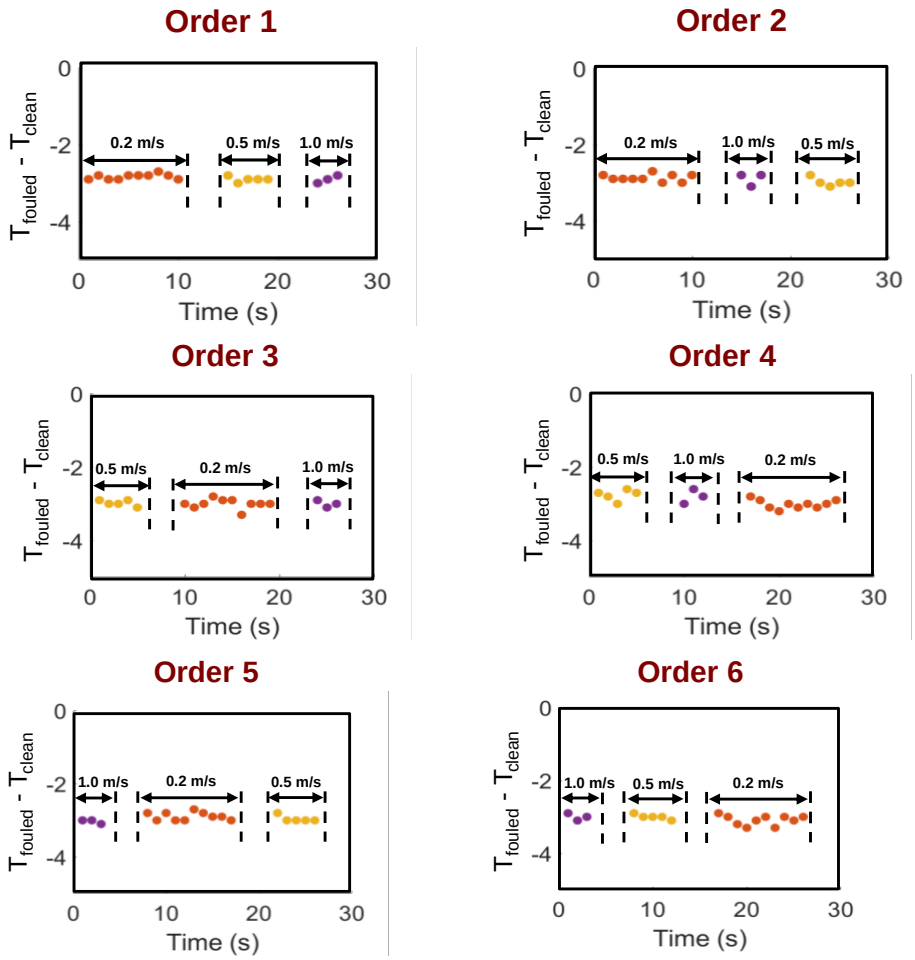

Figure 22 The temperature of fouled ballast compared with clean ballast measuring at three speeds in six different orders

Validating the Temperature Difference with The Application of Thermocouples

In this part, thermocouples are applied to measure the thermal behavior of the ballast. The thermocouples have the advantage of low cost, fast and relatively accurate temperature measurement. Most importantly, multiple thermocouples can be easily connected with the data acquisition device, which enables us to measure the temperature at different layers at the same time. The schematic diagram of the railroad ballast is given by Figure 23, which includes the track, sleeper, ballast, sub-ballast and sub-soil. The track and sleeper will block the natural convection on the ballast from the horizontal direction. And sometimes the sub-ballast layer and sub-soil layer could be considered as one layer, which is a mixture of finer particle and soil base.

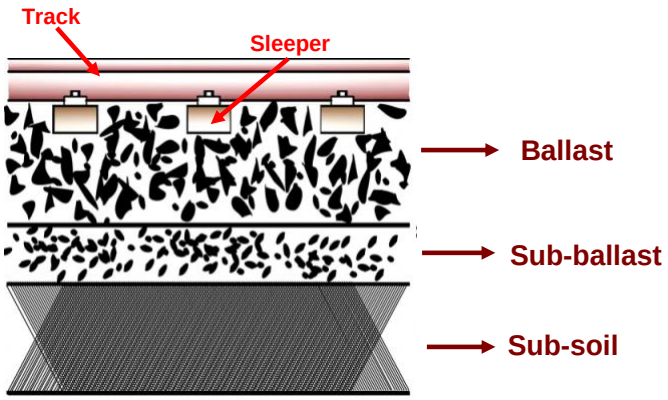

Figure 23 Schematic diagram of railroad ballast

To simulate what is happening in the field, we place wood blocks on top of the container to block the wind. As shown in Figure 24, on the top are the woodblock functioning as track, blocking the wind from the horizontal direction. The length of the woodblock is 31.5 inches. Below is the woodblock functioning as a sleeper, which blocks the wind from the side. The depth of the simulated sleeper is 6 inches. And on the bottom is the 11-inch-deep steel box used for containing the ballast.

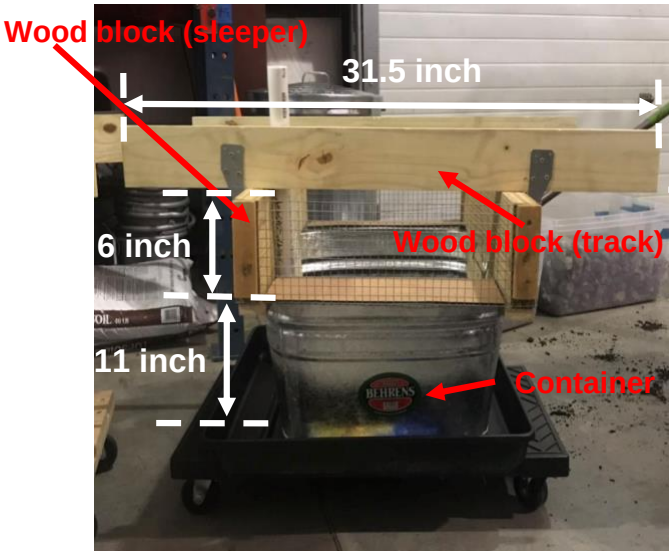

Figure 24. Experiment setup

In the container, pebble stones are used at the bottom layer as a base for water drainage, as shown in Figure 25 (a). The container is sealed on the bottom and thus the water is not able to flow through, which provides us the convenience of controlling the moisture content in the test setup. On top of the pebble stones, a 3-inch-deep layer of soil is placed to simulate the sub-soil layer. As shown in Figure 25 (b). Finally, the 12-inch deep ballast is placed on top of the soil base, as shown in Figure 15.

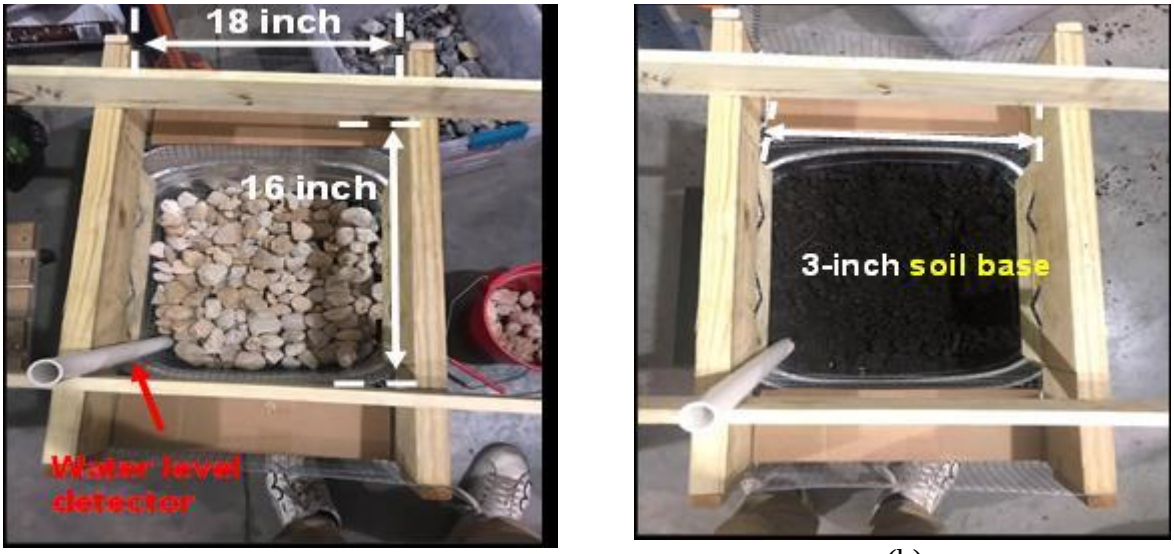

(a) (b)

Figure 25. The bottom layer of test setup: (a) pebble stone; (b) soil base

Figure 26. 12-inch deep ballast layer

Pre-Test: Analyzing the Effectiveness of the Proposed Experiment Setup

To study the thermal behavior of ballast at various depth, thermocouples are placed at the top surface, 2-inch,4-inch, 6-inch, 8-inch deep layer. Each layer 3 thermocouples are placed to minimize the random error. Before the actual experiment, a pre-test is conducted to see if all the thermocouples can provide similar temperature readings at each layer. In the pre-test, two containers are filled with clean ballast and fouled ballast, respectively. The fouling ratio of fouled ballast is 50% of the weight of the ballast. Generally speaking, the weight of the fouled ballast is much heavier than the clean ballast because of the fouling material. In our test, the fouling material is chosen as the topsoil that could be found in Home Depot. Notably, in this test, all clean and fouled ballast is dry, thus the effect of water is not considered.

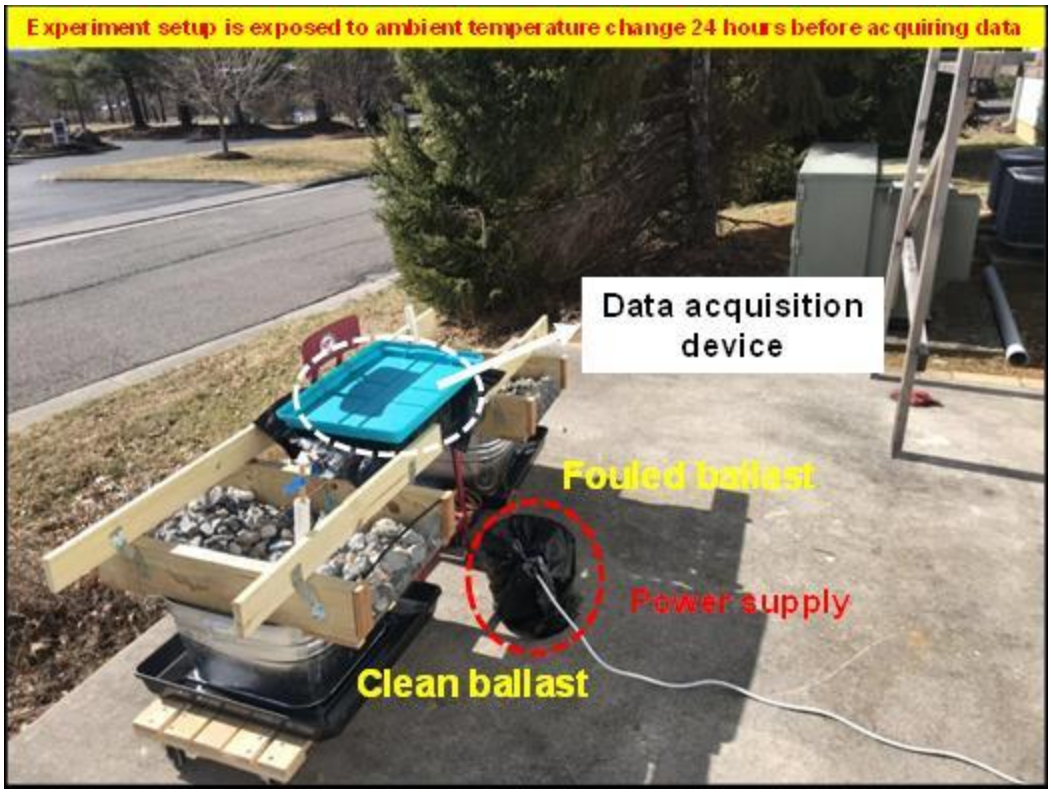

Figure 27. Pre-test with clean and fouled ballast placing side by side

The test result for the clean ballast is shown in Figure 17. In each sub-figure, temperature readings from three thermocouples are plotted with the ambient changing over time. The thermopiles are placed from the top surface to 6-inch deep. It could be observed that the thermocouples placed at 2-inch, 4-inch and 6-inch deep layers show good agreement with each other. It is indicated that the mean temperature of the ballast layer could be represented by these three thermocouples. However, for the ballast on the top surface, the three thermocouples show a great difference, for that the temperature measured by thermocouple #1 is much lower compared to the other two. Further, analyze is conducted to see why this is happening, and the reason is simply that, the woodblock generates shadow area, and #1 is in that area while #2 and #3 are not. That is the reason why #1 is not heating up fast. To avoid this inaccurate measurement, the three thermocouples should always be placed in the central area to minimize the influence of the shadow. Another interesting thing that could be observed from figure 28 is that the ballast on the top surface is much more sensitive compared to the ballast at lower layers. Similarly, the ballast at lower layers seems to be more stable.

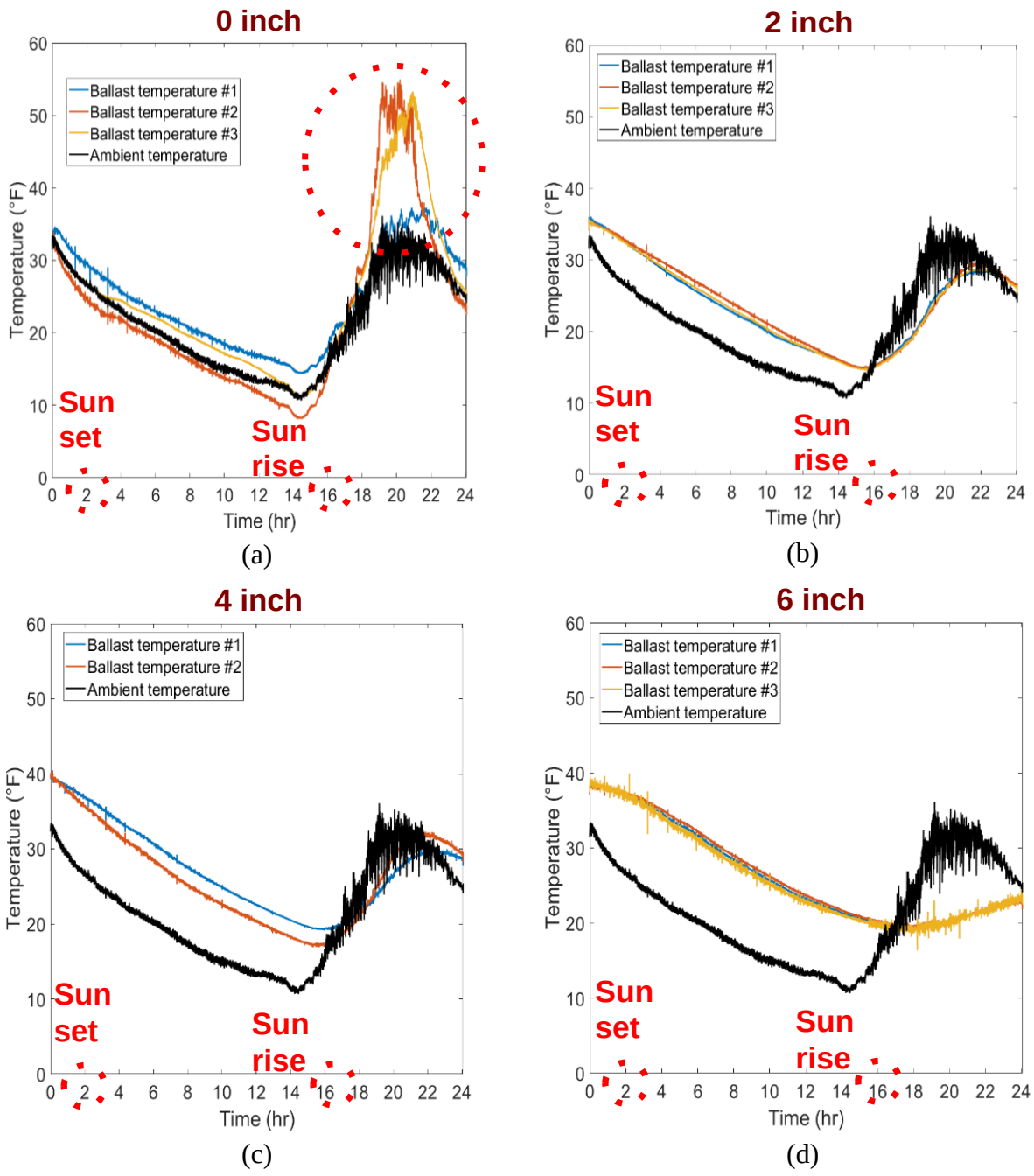

Figure 28. Temperature reading for clean ballast at different layers (test started at 4 pm)

The test result for the clean ballast is shown in Figure 29. Similarly, in each sub-figure, temperature readings from three thermocouples are plotted with the ambient changing over time. The thermopiles are placed from the top surface to 6-inch deep. The same pattern is observed, with the fact that the thermocouples placed at 2-inch, 4-inch, and 6-inch deep layers show good agreement with each other. Similarly, the temperature reading on the top surface shows that shadow has a major influence on the temperature reading. It could be observed that the thermocouple #1 peaks at nearly 70 degrees while the #2 and #3 peaks at less than 60 degrees. Also, it could be observed

that the ballast at deeper tends to be more stable.

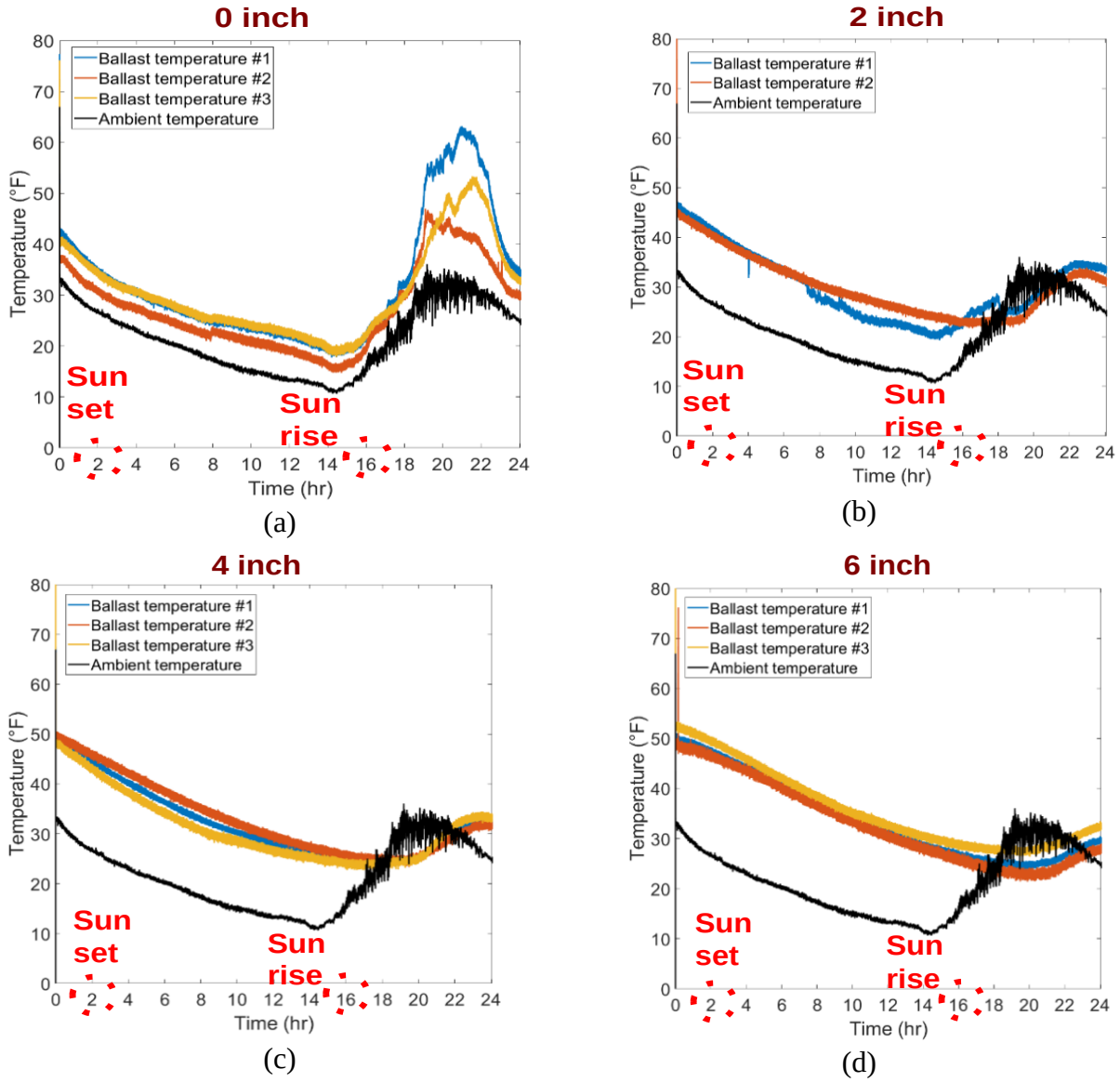

Figure 29 Temperature reading for fouled ballast at different layers (test started at 4 pm)

The effectiveness of the thermocouples is validated by the pre-test. In the following tests, thermocouples are placed from the top surface to the 8-inch-deep layer. And tests are conducted under both sunny and cloudy weather conditions. For fouling conditions, we consider ballast fouling which distributes evenly in the voids of ballast, referring to 'fully fouled', with the fouling ratio at 50%. Also, we consider the ballast fouling condition where the fouling has not yet influenced the top surface of the ballast. In other ways, the top 25% of ballast is completely clean and the rest 75% ballast is fouled evenly with contaminants, with the fouling ratio at 50% by weight. Among those tests, the ballast is tested under dry and wet conditions. The wet condition is generated by letting the natural rainwater gets into the ballast. The experiment setup is shown in Figure 30.

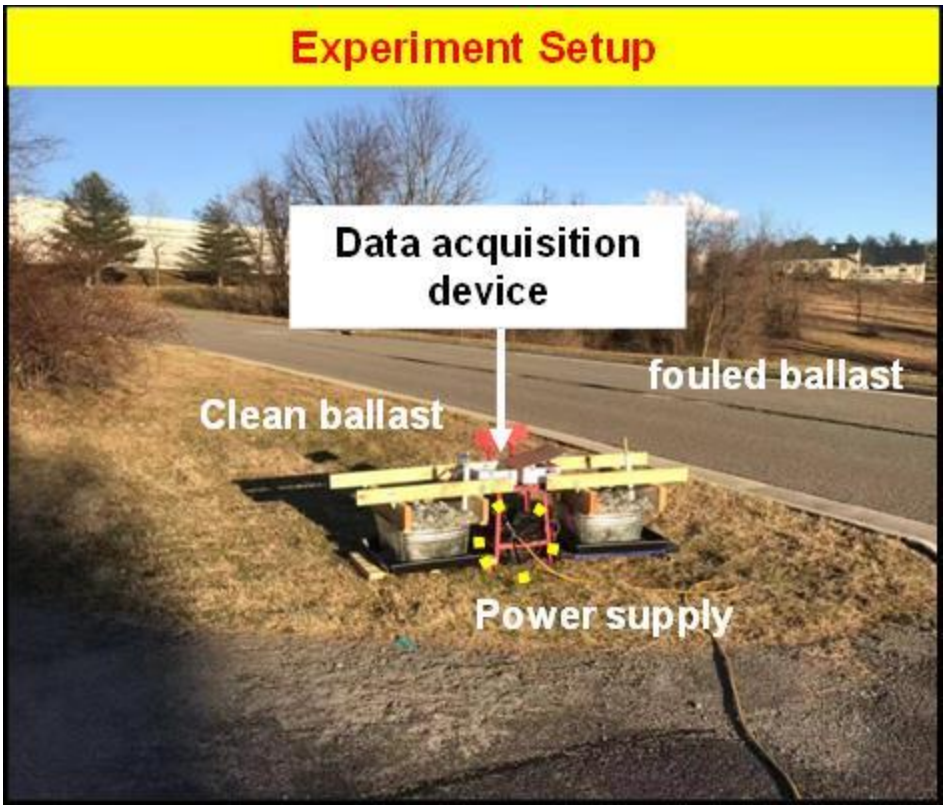

Figure 30 Experiment setup for outdoor tests

Test 1: Clean and 100% Fouled Ballast in Dry Condition

The test is to analyze the temperature difference between clean and 100% fouled ballast in dry conditions. All ballasts are dried by the natural wind and then applied for test purposes. The test setup is shown in Figure 30, where clean and fouled ballast are placed side by side exposing to naturally-occurring ambient temperature changes. The test was conducted on a sunny day, thus referring to "strong solar radiation". Similar to the pre-test, three thermocouples are placed at each layer of the ballast. Those layers include a surface layer, 2-inch-deep, 4-inch-deep, 6-inch-deep, and 8-inch-deep layers. Also, one thermocouple is used to measure the ambient temperature close to the ground. In total, 31 thermocouples are used in this experiment. Two data acquisition devices are used for collecting temperature data from the clean and fouled ballast.

The temperature at each layer is calculated by the average temperature reading of the three thermocouples placed on that layer. Figure 31 shows the mean temperature of each layer of clean ballast, where the black dashed line represents the ambient temperature changes during the test. It is obvious that the blue line, which is the temperature on the top surface is highly influenced by the ambient temperature or solar radiation. While for ballast at deeper layers, they seem to be less sensitive. For ballast at the 8-inch-deep layer, the temperature fluctuation throughout the daily based ambient environment changing cycle is minor.

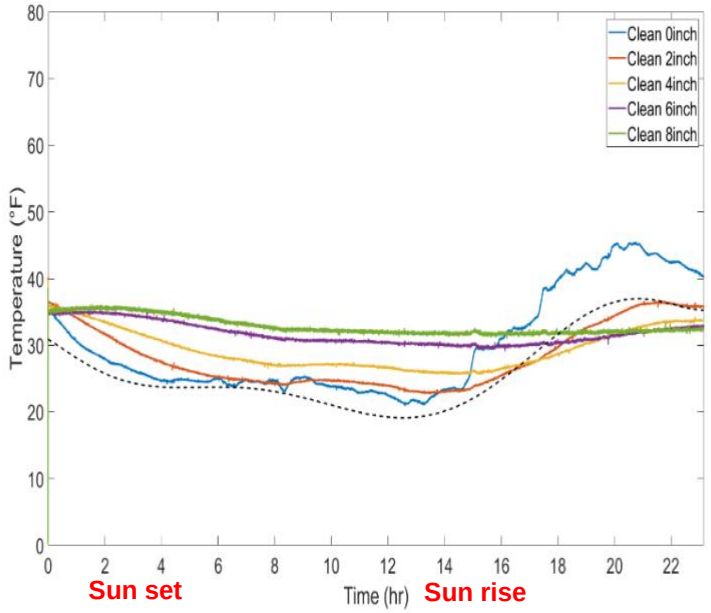

Figure 31 Temperature reading for fouled ballast at different layers (test started at 4 pm)

A similar pattern is observed for fouled ballast, which is shown in Figure 32. It is obvious that the blue line, which is the temperature on the top surface is highly influenced by the ambient temperature or solar radiation. While for ballast at deeper layers, they seem to be less sensitive compared to the ballast on the top surface. Notably, the random noise observed in this test is higher than that of the clean ballast. The reason is unsure but should have something to do with the fouling contaminant in the ballast voids.

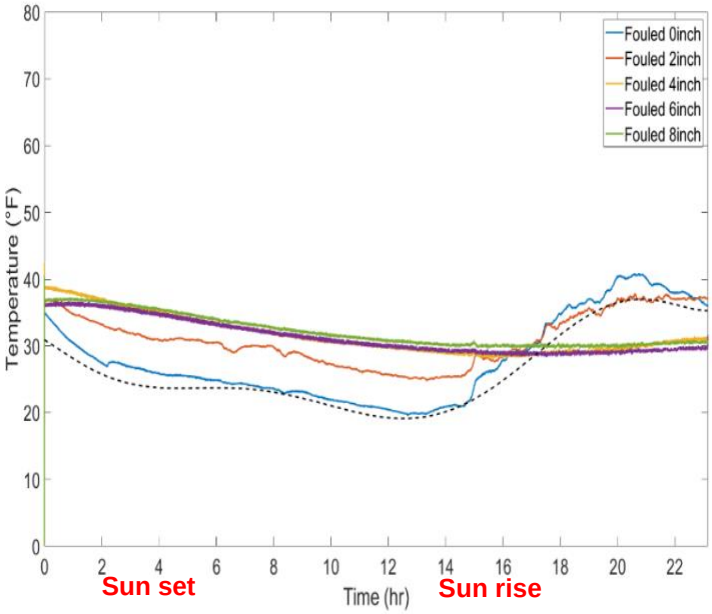

Figure 32 Temperature reading for fouled ballast at different layers (test started at 4 pm)

To compare the difference between clean and fouled ballast, their temperature difference is calculated as shown in Figure 33. For all layers, the temperature difference is minor. Notably, the temperature difference peaks at 2 and 4-inch-deep ballast. This is because the top 4-inch layers of ballast allow the flow of natural convection. For deeper layers like 6 and 8-inch deep, there is no obvious temperature difference throughout the experiment.

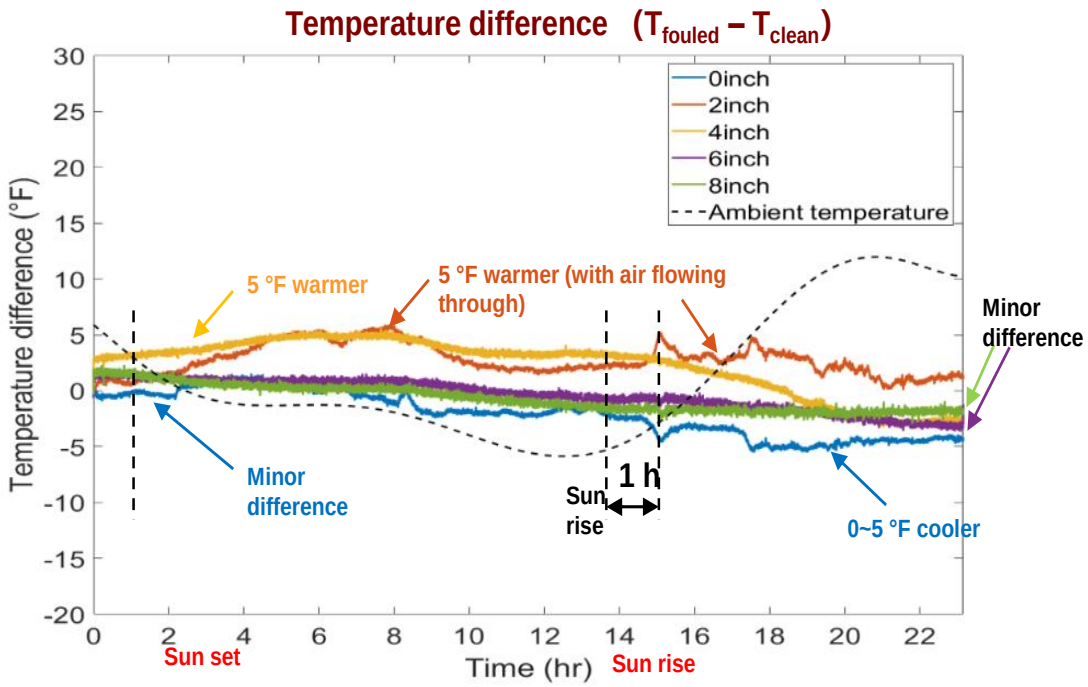

Figure 33 Temperature reading for fouled ballast at different layers (test started at 4 pm)

Test 2: Clean and 100% Fouled Ballast with the Participation of Water

Ballast fouling usually associates with retained water, because the contaminants will block the water passage and thus make the fouling worse. So in test 2, the influence of water is taken into consideration. The test setup is identical to that of test 1, where clean and fouled ballast are placed side by side exposing to naturally-occurring ambient temperature changes. The same amount of water was added to both ballasts. The experiment begins when all water sinks into the void of ballast. We notice that the clean ballast is not able to hold water and thus water drain away fast, while the fouled ballast is quite the opposite.

Figures 34 and 35 show the temperature at different depth of clean and fouled ballast. The conclusion is similar to that of test 1, where the ballast on the surface is found to be much more sensitive to ambient temperature changes for both ballasts.

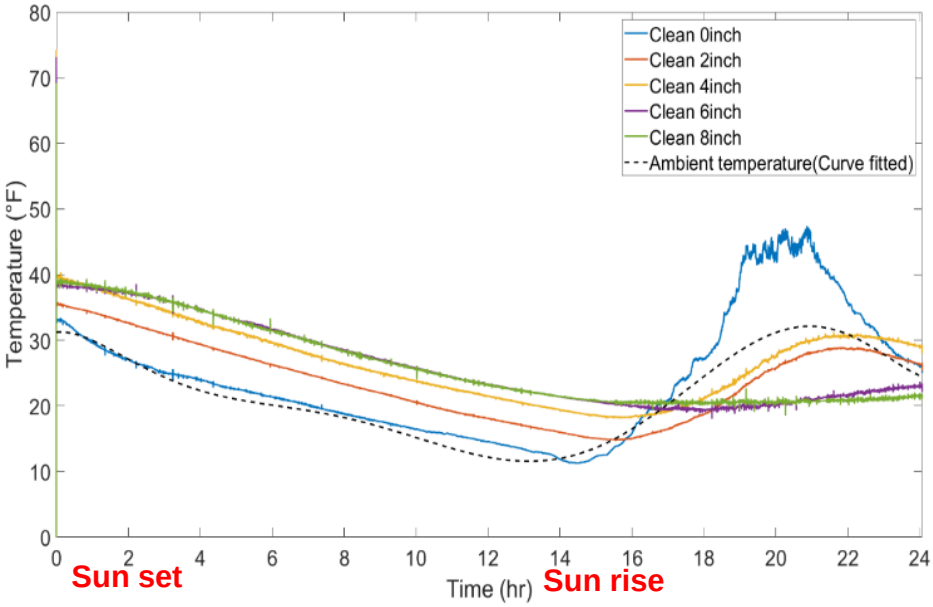

Figure 34 The mean temperature of clean ballast at various layers (test started at 4 pm)

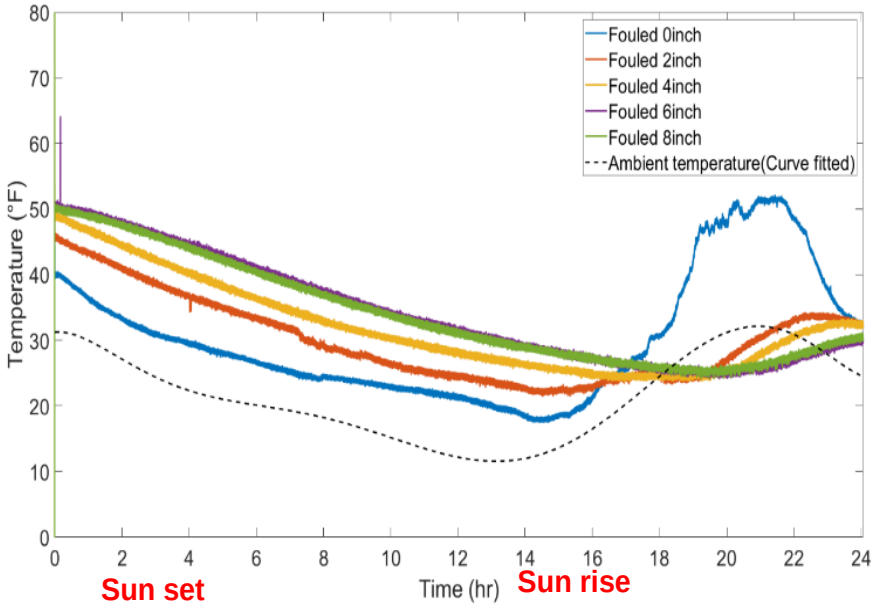

Figure 35 The mean temperature of fouled ballast at various layers (test started at 4 pm)

In order to compare the difference between clean and fouled ballast, the temperature of each layer is calculated as shown in figure 36. The figure provides a lot of information. First of all, during the night, all layers of fouled ballast are warmer than clean ballast. The difference on the surface is around 5 degrees and the difference increase for deeper layers, which is approximately 10 degrees. Also, after the sunrise, the ballast at deeper layers reacts slower to the ambient temperature changes, because of the fact that solar radiation affects the surface directly, and the heat conduction between ballast is much less efficient compared to the radiant heat transfer. Lastly, a peak of around 20 degrees is observed on the surface, which is mainly because of the shadow. This also

indicates the fact that three thermocouples are barely enough to represent the temperature of a layer of ballast. For further experiments, a matrix of thermocouples should be used, but this also increases the complexity of the test setup dramatically.

To draw a conclusion, a difference is observed between the clean and fouled ballast. On the surface, the difference is around 5 degrees and on a deeper layer, a larger difference of 10 degrees is observed.

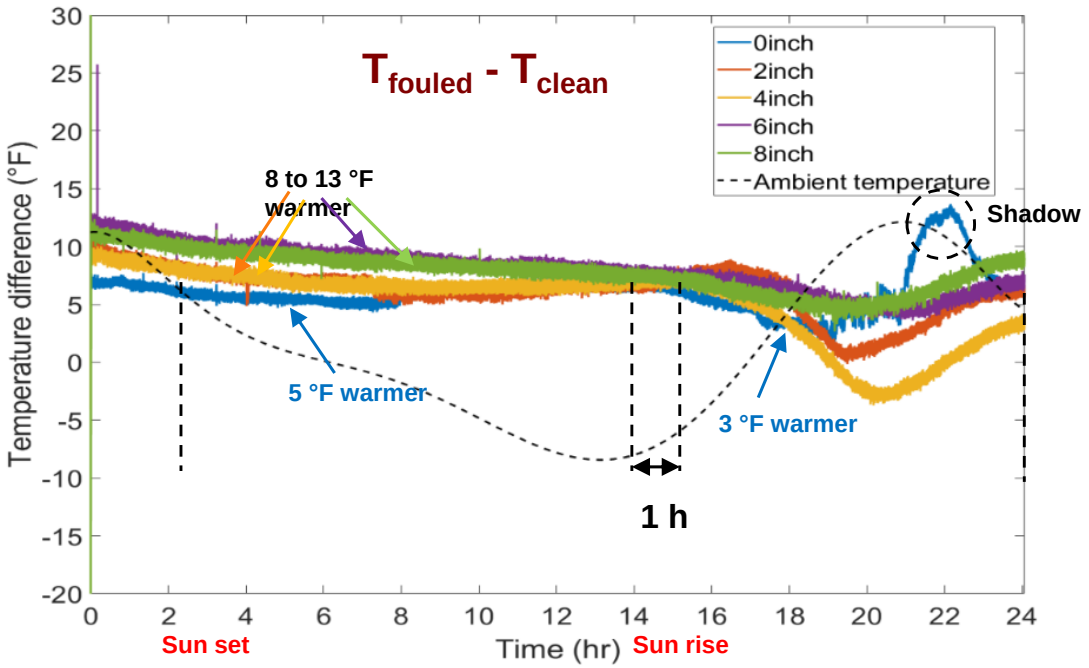

Figure 36 The temperature difference between clean and fouled ballast (test started at 4 pm)

Test 3: Clean and 75% Fouled Ballast without Water

During the process of fouling, the ballast is not always fully fouled, which indicates a mixture of air void, particle ballast, and fouling material. The ballast that is a mixture of clean and fouled ballast is referred to as 'partially fouled ballast'. In test 3, we compare the thermal difference between clean and partially fouled ballast. The top 25% of ballast is clean and the rest ballasts are fouled ballast, with a fouling ratio of 50%. The experiment setup is identical to that of former tests. The temperature results for clean and fouled are shown in Figures 37 and 38 respectively. A similar pattern is observed that the deeper ballast is less sensitive to the ambient temperature changes.

The temperature difference is shown in Figure 39. It indicates that, during the night, there is no temperature difference between clean and partially fouled ballast at all depths. However, during the day, it shows a clear difference, especially at the top surface, with a difference of more than 10 degrees. This difference shows that during daytime, the partially fouled ballast is likely to achieve a higher temperature.

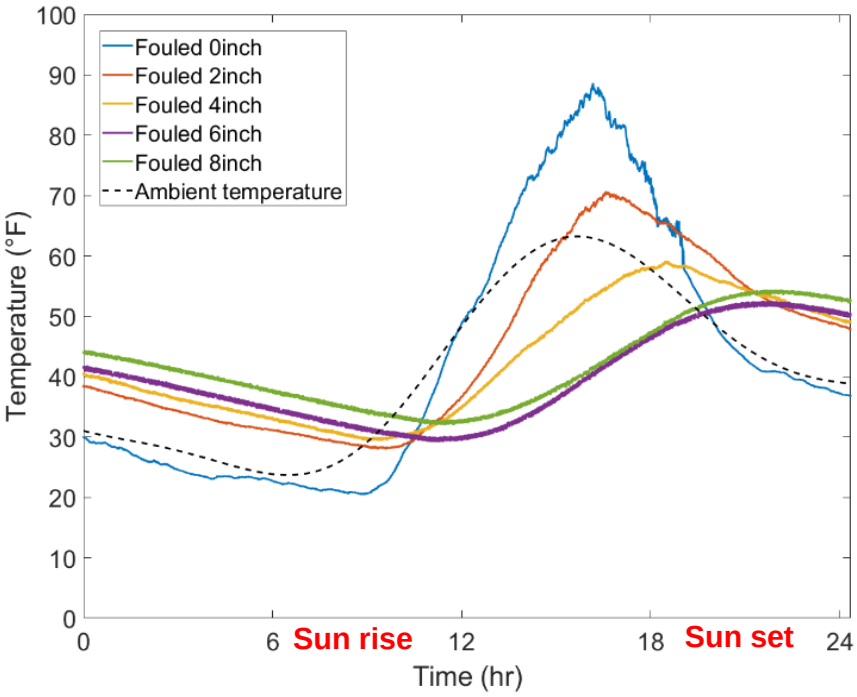

Figure 37 The temperature difference between clean and fouled ballast (test started at 10 pm)

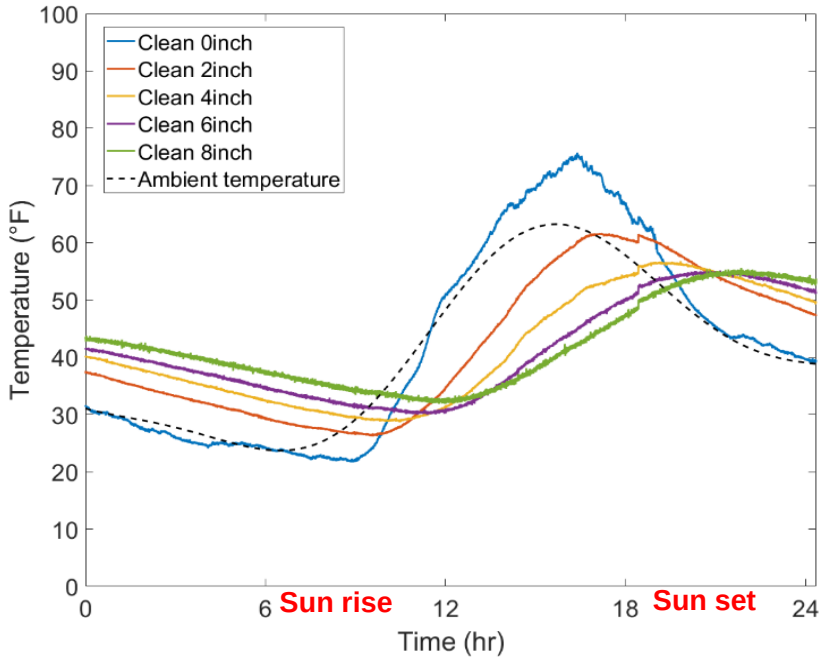

Figure 38 The temperature difference between clean and fouled ballast (test started at 10 pm)

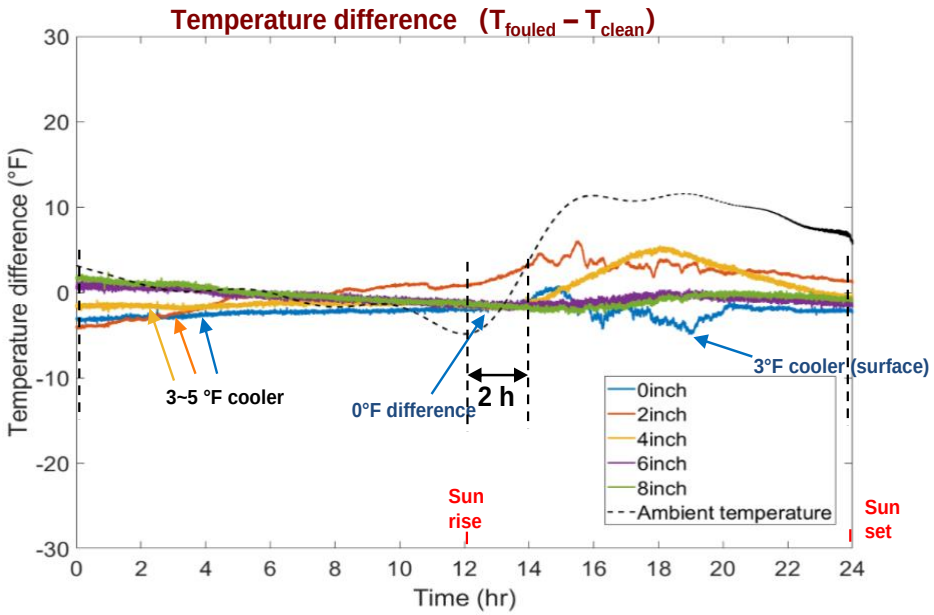

Figure 39. The temperature difference between clean and fouled ballast (test started at 6 pm)

Test 3: Clean and 75% Fouled Ballast with Water

Based on the result obtained from Test 3, a further test is conducted with the participation of water. Similar to Test 2, water is added into both ballasts, and then drained away freely. The temperature difference is observed shows the plot of temperature difference, as shown in Figure 40. It is shown that there is a minor temperature difference between clean and partially fouled even with the participation of water.

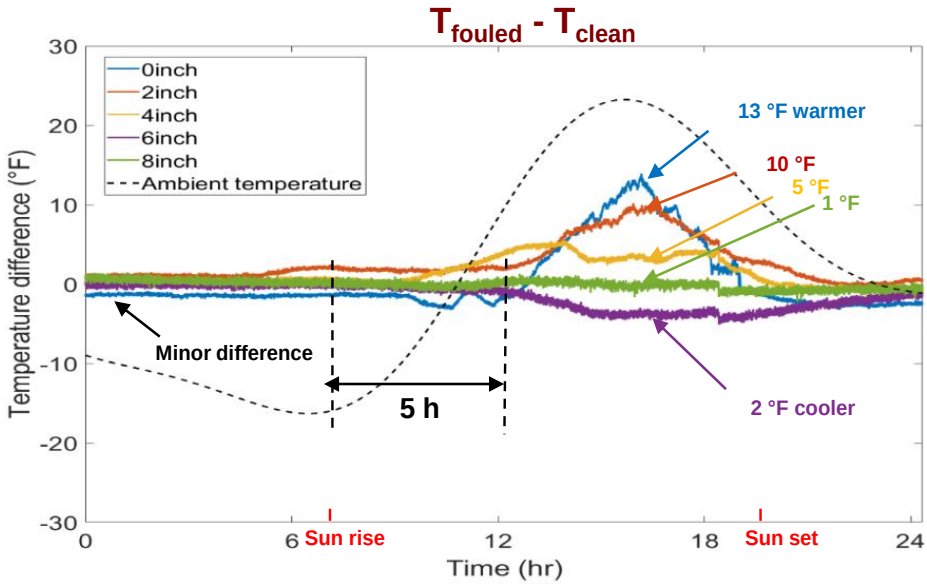

Figure 40 The temperature difference between clean and fouled ballast (test started at 10 pm)

To draw a conclusion from Tests 1, 2, 3 and 4, all tests show that the surface ballast is more sensitive than deeper layers. Also, the temperature difference is observed for clean and fully fouled ballast with the participation of water, where on the top surface there is a 5-degree temperature difference, and on the deeper layers, there is a proximately 10-degrees difference. Also, the temperature difference is observed for the clean and partially fouled ballast. However, the difference is observed during the day instead of during the night. This difference could likely be caused by the shadow or caused by the thermocouples. In general, a large temperature difference is only observed for the clean and fully fouled ballast with the participation of water. This limits the application of the FLIR camera because of the measurement accuracy is relatively low for this range of temperature difference.

To further analyze the thermal behavior of the ballast, the numerical model is built for ballast in the next chapter.

MODELING AND SIMULATION STUDY OF BALLAST

In this part, a numerical model is developed based on one-dimensional conductive heat transfer of railroad ballast. The effort is made to experimentally validate the numerical model, with the application of thermocouples measuring the temperature at various depth of ballast in an indoor experiment setup. The experiment result shows good agreement with the simulation results. Simulations are later carried out to analyze the thermal behavior of ballast with different amounts of contaminants and water. Different thermal behavior is observed for ballast at different layers and under different conditions. Conclusions are drawn by analyzing both temperature and temperature difference between those ballasts.

A Numerical Model of Ballast

Analyzing the thermal behavior of the ballast regarding the fouling process under various environmental conditions is the objective of this paper. The one-dimensional numerical model is proposed based on one-dimensional combined convective and conductive heat transfer, where the radiant heat transfer inside the ballast is also considered. The developed model assumes as follows:

- The ballast is regarded as a homogeneous material composite of ballast, air and fouling material
- Local thermodynamic equilibrium is assumed between all phases
- The thermal property of the material is independent of the temperature and time
- The natural convection inside the ballast is ignored due to the slow airflow

The governing energy balance equation for heat transfer of ballast is written as follows:

$$(1-\varphi)(\rho_s C_s)\frac{\partial T}{\partial \tau} + (\varphi * (1-F))(\rho_a C_a)\frac{\partial T}{\partial \tau}) + (\varphi * F)\left(\rho_f C_f\right)\frac{\partial T}{\partial \tau} = k\frac{\partial^2 T}{\partial x^2} \quad (1)$$

where φ is the porosity of bulk ballast, T temperature, τ time, x is the depth of ballast layer, F the fouling ratio, ρ and C the density and specific heat capacity. The subscript s denotes solid particle of ballast, a the air, f the fouling material.

The fouling ratio is calculated as the ratio of the volume of voids in ballast to the volume of contaminants present in the ballast (fouling material). It is measured in percentage:

$$F = \frac{V_2}{V_1} * 100\% \quad (2)$$

Here V_2 is the volume of voids in the ballast and V_1 is the volume of contaminants in the ballast. According to (Tan et al. 2019), the porosity of the clean ballast is relatively high thus the radiant heat transfer between the ballast should be taken into consideration. However, the calculation of radiant heat transfer inside the ballast is very computational expensive because it's not only a function of distance and temperature of all ballast. To simplify the calculation process, (Hosseini et al. 2020]) simplified the radiant heat transfer as a diffusion process, and its contribution could be further calculated in the form of conductive heat transfer (Shen et al. 2007). In analogy to thermal conductivity, the measure of its ability to transfer heat is called radiant conductivity. The

overall conductivity is defined as the sum of thermal conductivity and radiant conductivity, which is given as follows:

$$k = k_t + k_r \tag{3}$$

where k_t and k_r are thermal conductivity and radiant conductivity, respectively. For porous medium, they are further given by Gatmiri and Delage (1997) and Choi et al. (2013):

$$k_t = \frac{(k_{2p}k_s - k_a)(1-\varphi) + k_a}{1 + (k_{2p} - 1)(1-\varphi)} \tag{4}$$

$$k_r = \frac{4d\sigma T_m^3}{3} \tag{5}$$

Where φ is the porosity of ballast, k_a is the conductivity of particle ballast and pore air, d is the mean distance between ballast, σ is a constant and T_m is the local mean temperature. k_{2p} is a function of the conductivity of solid particle of ballast and conductivity of air, which is further given by

$$k_{2p} = 0.29\left(\frac{k_s}{k_a}\right)^{p} \tag{6}$$

where φ is the porosity of ballast, k_a is the conductivity of particle ballast and pore air, d is the mean distance between ballast, σ is a constant and T_m is the local mean temperature.

The physical system is modeled as a one-dimensional system with adiabatic side boundaries. The top layer is radiation boundary and the bottom layer is assumed to be at a constant temperature. The boundary condition is summarized in the following equations:

$$(\rho C)\frac{\partial T}{\partial \tau} = R(t) - \varepsilon\sigma\left(T^4 - T_a^4(t)\right), x = 0 \tag{7}$$

$$(\rho C)\frac{\partial T}{\partial \tau} = \ T_{ave}, \qquad x = L \tag{8}$$

Equation (7) represents the energy exchange between the top surface and ambient temperature. $R(t)$ is the radiation power absorbed by ballast, ρ, and C are the density and specific heat capacity of bulk ballast, T_a is the ambient temperature. Equation (8) represents that the bottom layer is at a constant temperature, which is the average ambient temperature throughout the simulation cycle.

Validation of the Proposed Model by Indoor Experiment

The proposed model is verified by an indoor experiment setup for clean and fouled ballast, using the field-collected ballast sample. To formulate 'clean ballast', all samples are washed by clean water and dried up to avoid any water content. Part of the samples is further mixed with dry soil to formulate 'fouled ballast', where the weight of fouling material is half of the clean ballast. The porosity of clean ballast is 48%, which is estimated by measuring the volume of water present in

the saturated sample. The bulk density of clean and fouled ballast is 1590 and 2345 Kg/m3 respectively, which is directly calculated by measuring their bulk volume and weight. And the specific heat capacity of clean and fouled are 429 and 672 J.Kg-1.K-1, calculated by adding up the specific heat capacity of ballast, air and fouling material by their percentage. The conductivity of clean and fouled ballast is 0.38 and 0.54 W.m-1.K-1, which are calculated by the equation given in Gatmiri and Delage (1997) where the conductivity of particle ballast and fouling material are chosen from related research work (Andre and Degiovanni 1995).

The ballast sample is placed in a wooden container. The inside of the container is covered with a thermal isolator to block the heat transfer on the side of the ballast. Four heating lamps are used to format a uniform radiation heating source on the top surface of the ballast. An optical power meter is used to measure the radiation power on the surface. The radiation power ranges from 280 to 310 W/m2, and its mean value of 301 W/m2 is used as the radiation power for the simulation.

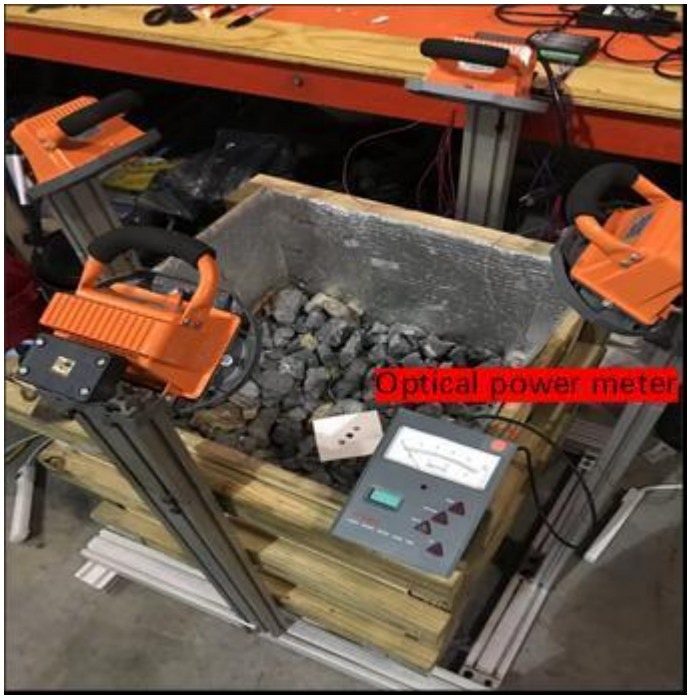

Figure 41 The experiment setup of the indoor test

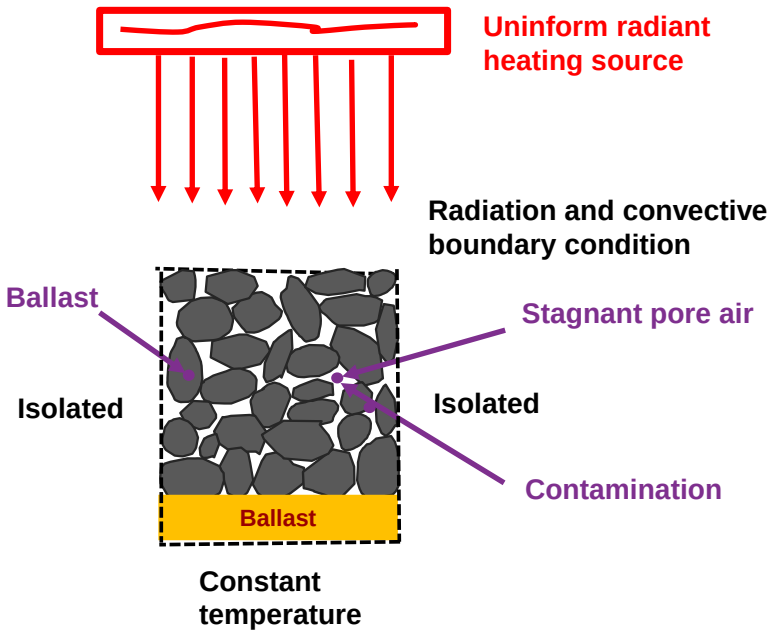

Figure 42. Schematic experiment setup

In practice, the radiation power that reached the surface is not completely absorbed by the ballast. To measure the absorption ratio of ballast to the heating lamp used in the experiment, the integrating sphere is used to measure the reflectivity of five ballast samples. The integrating sphere is an optical component consisting of a hollow spherical cavity with its interior covered with a diffuse white reflective coating, with small holes for the entrance of light and exit ports. The light on any point on the inner surface is, by multiple scattering reflections, distributed equally to all other points. Thus, the reflected light could be measured by the detector. The raw reflectance and relativity reflectivity are given in the following table. The mean value of 80.2% is used to calibrate the energy absorbed by the surface layer of the ballast.

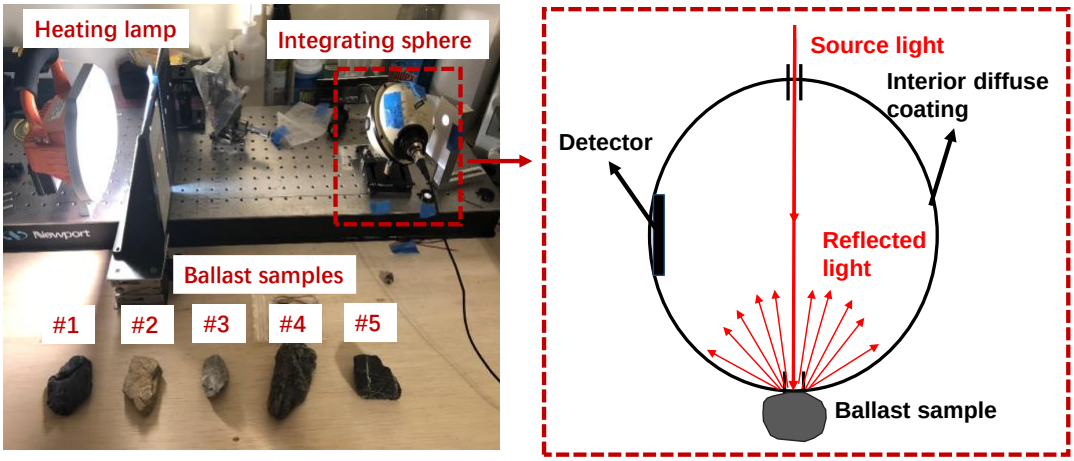

Figure 43 Test setup for measuring the reflectance of ballast

Table 1. Reflectance Value of Ballast

Rock	*Raw reflectance*	*Reflectance (%)*
#1	0.344 mw	5.17%
#2	0.448 mw	32.04%
#3	0.435 mw	28.69%
#4	0.350 mw	6.72%
#5	0.345 mw	5.43%

Thermocouples are used to measure the temperature at various depths of ballast. In order to ensure good contact patch between ballast and thermocouples, each ballast is drilled with an approximal 0.5 cm deep hole, and the head of thermocouples are then fixed in the openings, as shown in figure 44. The thermocouples are connected with ballast and then placed on the surface, 2-inch deep and 4-inch deep layer respectively. Five thermocouples are placed on each layer to minimize the random error caused by single-point reading and avoid the non-uniform temperature distribution caused by the boundary effect.

1. 

2. (a)

3. 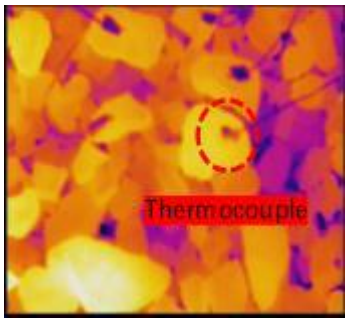

4. (b)

Figure 44 (a) Thermocouple embedded on the surface of the ballast. (b) Multiple thermocouples placed on each layer (thermal image)

Before the experiment, all ballast samples are given enough time to reach the thermal equilibrium of environmental temperature, which is nearly constant at 74 degrees Fahrenheit. The experiments start with turning on four heating lamps to heats up the ballast for one hour, and then the heating lamp is removed to allow the ballast to cool down naturally for another two hours.

To validate the effectiveness of the proposed model, the exact same radiation power and ambient temperature are applied for the simulation, which is shown in Figure 45. The measured and calculated thermal characteristics such as bulk density, specific heat capacity and conductivity are also used in the simulations.

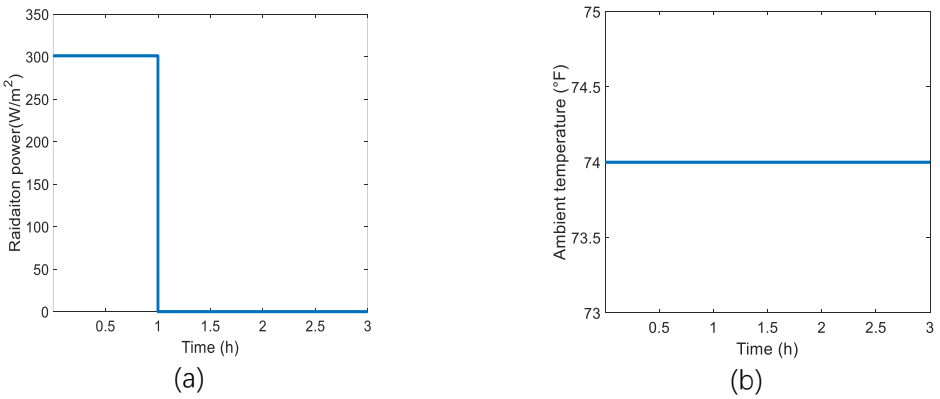

Figure 45 (a) radiation power. (b) ambient temperature

Figure 46 shows the comparison between the experimental and simulation result for clean ballast. For ballast at all three depths, the experiment result agrees well with simulations results. In the first hour of the experiment, the ballast on the top surface is significantly heated up from 74 degrees Fahrenheit to 140 degrees Fahrenheit, while the temperature of the ballast at 2-inch depth only increases by 5 degrees Fahrenheit and ballast at 4-inch depth only increases by 2 degrees. The heating source is then removed in the rest two hours of the experiment. It is observed that the ballast on top surface cooling down immediately, while it takes 0.5 hours for the 2-inch-deep ballast to start to cool down. Interestingly, the 4-inch deep ballast is stilled heating up even two hours after removing the heating source, although a lower temperature changing rate is observed.

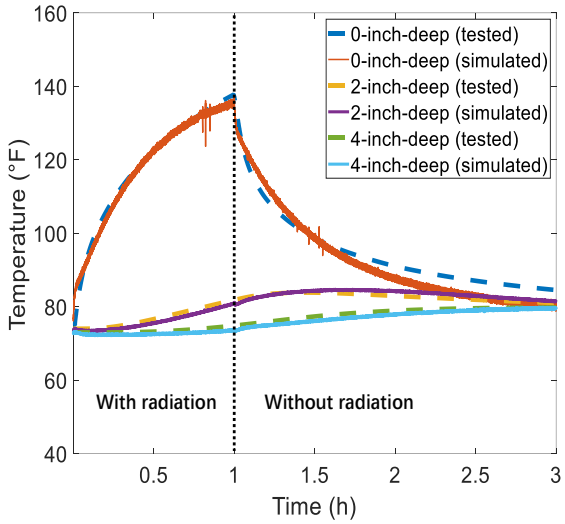

Figure 46 Comparison between simulation and experiment result of clean ballast

Figure 47 shows a comparison between the experimental and simulation result for fouled ballast. For the ballast on the top surface, the model under-estimate the peak temperature value by approximately 15 degrees, which might possibly because the added contaminants have a higher absorption ratio to the heating source. However, after the removal of the heating source, the predicted temperature agrees well with the experimental result. For ballast at deeper layers, the predicted result agrees well with the experiment result during both heating up and cooling down period. The thermal behavior of fouled ballast is similar to that of clean ballast, where the ballast

on surface heats up and cools down fast and the ballast at the lower layer is less sensitive to the changes of the ambient environment.

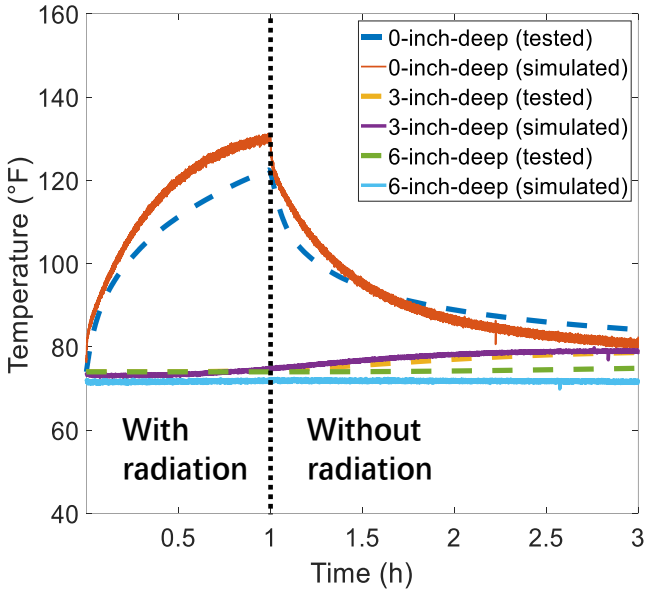

Figure 47. Comparison between simulation and experiment result of fouled ballast

In all, the effectiveness of the proposed model is validated by the indoor experiment for both clean and fouled ballast. Specifically, the thermal behavior of ballast at various depths and various ambient conditions is analyzed. In the next part, the proposed model is used to analyze the effect of fouling on the ballast under various conditions.

A Simulation Study of Ballast

In this section, two case studies are performed based on the proposed model to analyze the effect of fouling on the ballast. Case 1 studies the thermal behavior of ballast with different amounts of fouling at various depths. Comparisons are made between clean and fouled ballast. Case 2 further studies the thermal behavior of fouled ballast with the participation of water, where the thermal behavior at different depth is also analyzed.

Continues field-collected five-days ambient temperature and solar radiation power data are used for the purpose of the simulation. The data is obtained in the middle of the US in a typical winter by the national renewable energy laboratory (NREL). As shown in Figure 48, the 5-day environmental data includes the ambient temperature and solar radiation changes in different ranges, which provides the capability of analyzing the thermal behavior of ballast under different environmental conditions. Also, it could be observed that the ambient temperature and solar radiation are not directly related, which implies the advantage of using field-collected data instead of simulated environmental data.

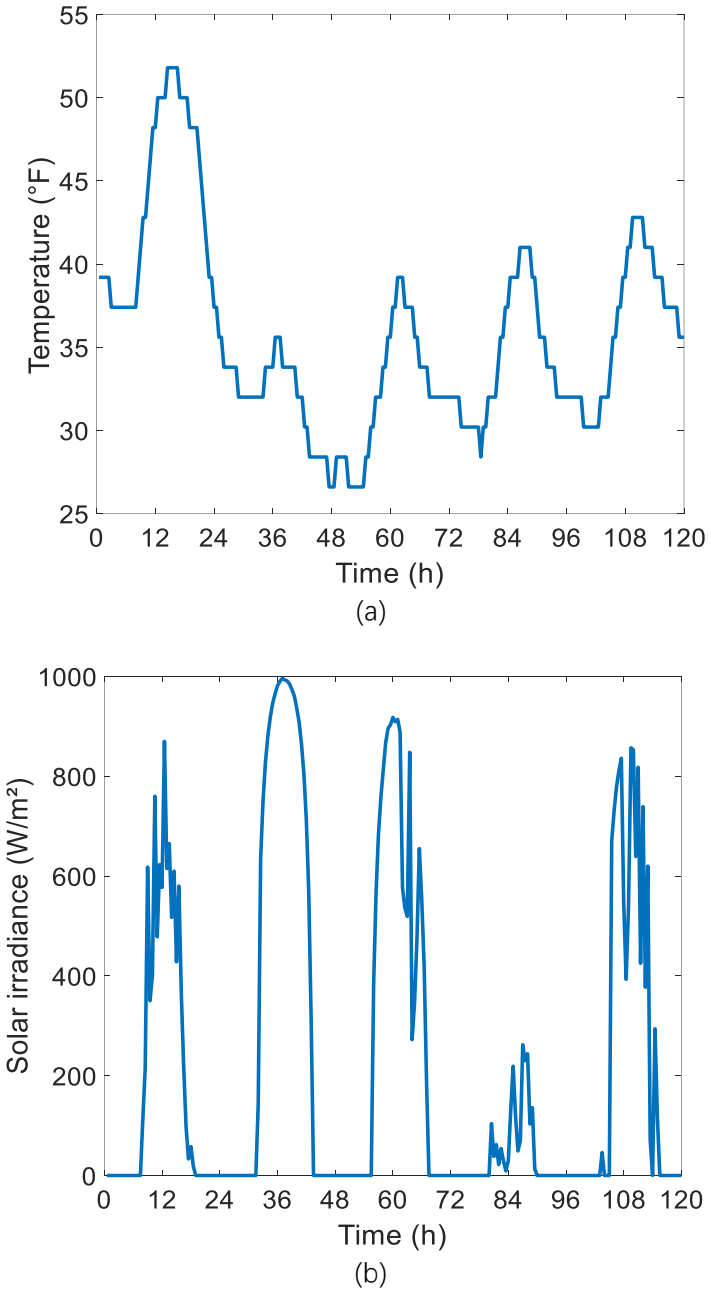

Figure 48. Five-day climate data from National Renewable Energy Laboratory (NREL): (a)Temperature (b) Solar irradiance

Case 1: The Effect of Fouling Ratio on the Thermal Behavior of Ballast In Case 1, the clean and fouled ballast samples are exposed to the ambient temperature and solar radiation given in figure 49. Fouled ballast is formulated by adding contaminants into clean ballast, where fouling ratio of 20%, 40%, 60%, 80%, and 100% are considered.

Figure 49 (a) to (d) shows the thermal behavior of clean and fouled ballast from the top surface to the 12-inch deep layer. It could be observed that ballasts at all depths are influenced by the environmental changes, while the ballast at a deeper layer is less sensitive. In (a), the ballast on the surface shows a temperature fluctuation of 40 degrees throughout the 120-hour cycle. For ballast at 4-inch and 8-inch deep layer, as shown in (b) and (c), a fluctuation of 20 and 10 degrees is observed, respectively. The ballast on the 12-inch deep layer is nearly constant throughout the simulation cycle, as shown by (d).

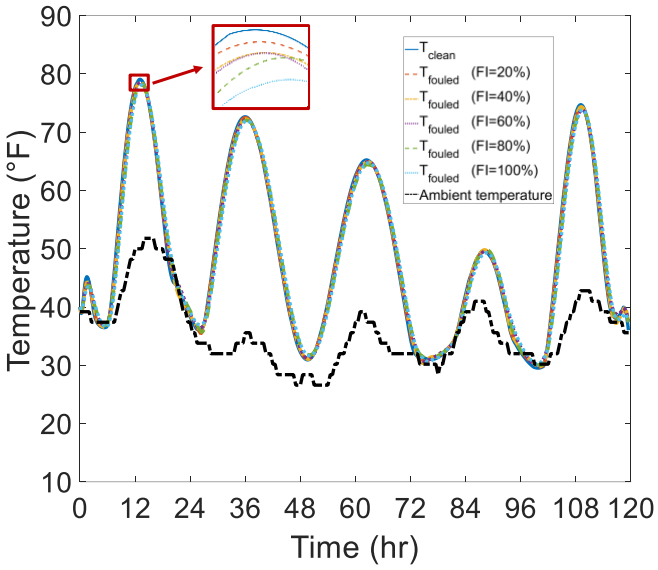

(a)

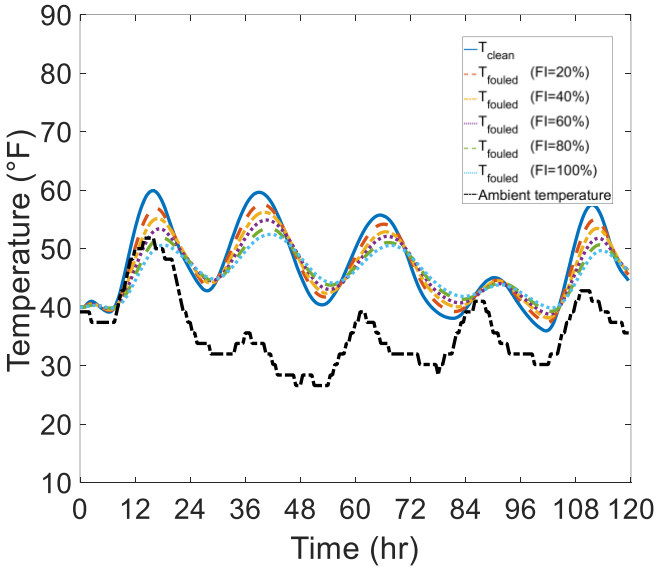

(b)

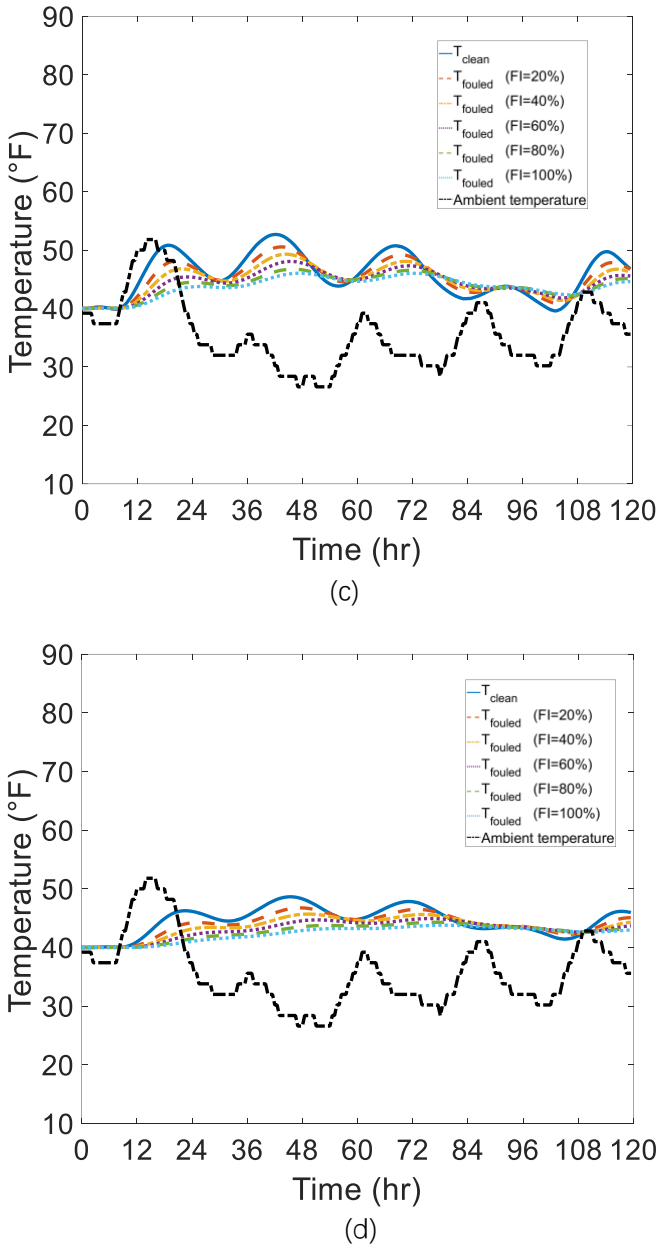

Figure 49. Comparison between ballasts with different fouling ratio: (a) At the surface layer; (b) At 4-inch deep layer; (c) At 8-inch deep layer; (d) At 12-inch deep layer

To compare the effect of fouling on the thermal behavior of ballast, the temperature difference between clean and fouled ballast is calculated and plotted at the surface, 4-inch, 8-inch, and 12-inch deep layers, as shown in Figure 50. A similar pattern is observed for ballast at all depths, which is that more amount of fouling results in a larger temperature difference between clean and fouled ballast. Specifically, figure 50a shows the temperature difference on the top surface, which is within 5 degrees. The temperature difference increases for the ballast at the 4-inch depth, in a range of 4 to 12 degrees. However, the temperature difference starts to decrease from the 4-inch deep layer. For ballast at the 8-inch deep layer, the temperature difference decreases to a range of

3 to 8 degrees. And for ballast at 12-inch depth, even less temperature difference is observed, in a range of 3 to 6 degrees. The simulation result indicates the thermal behavior difference increases from the top surface to the 4-inch deep layer and then decreases for ballast at a deeper layer. This reveals that when the ballast gets fouled, the maximum temperature difference is expected to be observed at the 4-inch deep layer.

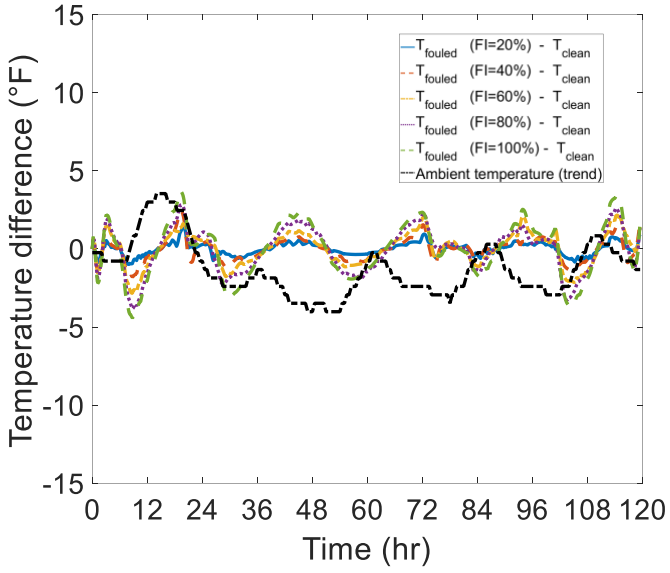

(a)

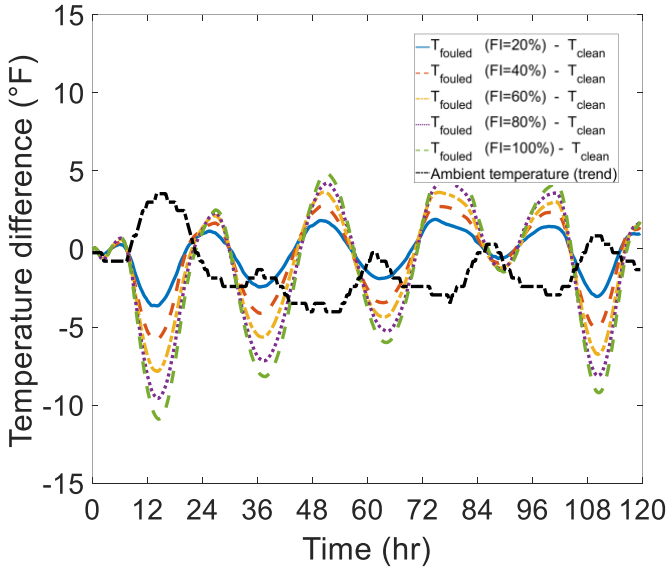

(b)

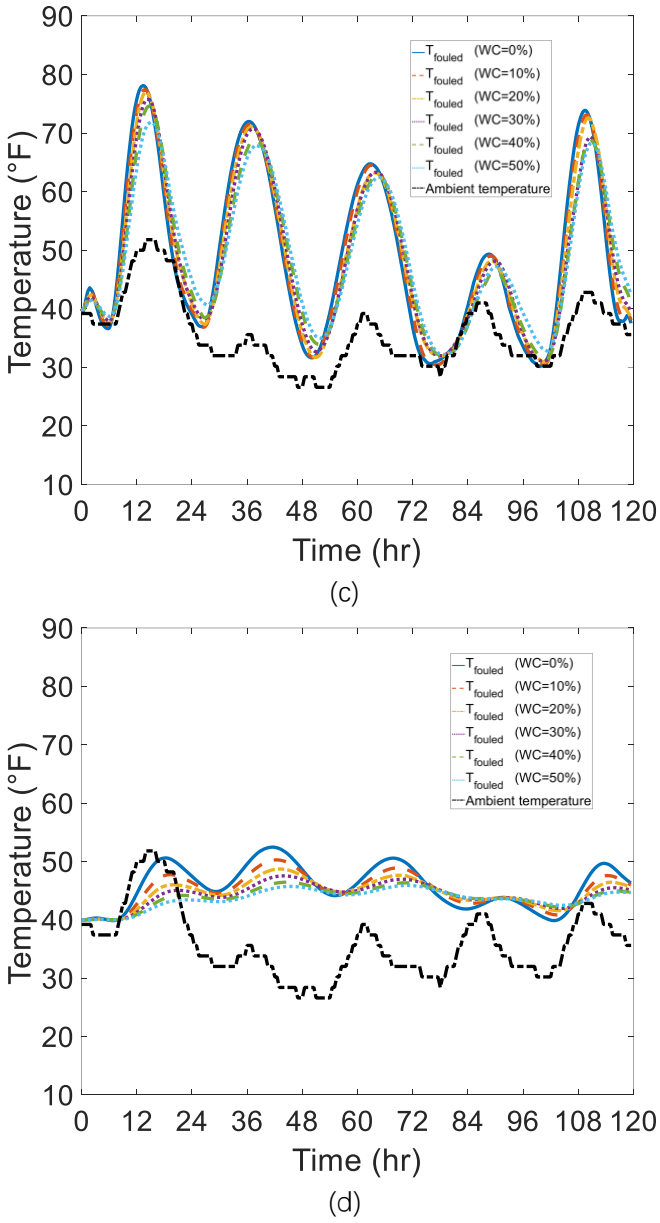

Figure 50. The temperature difference between the ballast with different fouling ratio: (a) At surface layer; (b) At 4-inch deep layer; (c) At 8-inch deep layer; (d) At 12-inch deep layer

Case 2: The Effect of Water on the Thermal Behavior of Ballast During the operation of the railroad, the contaminants will block the water drainage. To analyze the thermal behavior of the ballast under this condition, the influence of water needs to be considered. Here we choose the fouled ballast with 100% of fouling as our reference, and 10%, 20%, 30%, 40% and 50% percent of water is added.

Figure 51 (a) to (d) shows the thermal behavior of fouled ballast with different amounts of water from the top surface to the 12-inch deep layer. Similar to the pattern observed in case one, ballasts

of all conditions at all depths are influenced by the environmental changes, while the ballast at the deeper layer is less sensitive to those. In (a), the ballast on the surface shows a temperature fluctuation of 40 degrees throughout the 120-hour cycle. Also, the ballast with more water shows a delay when reacting to the ambient changes. For ballast at a deeper layer, the temperature fluctuation is reduced dramatically, as shown in (b), (c) and (d). Notable, for the ballast at 12-inch deep layer, the influence of daily environmental changes is nearly negotiable, as shown in (d).

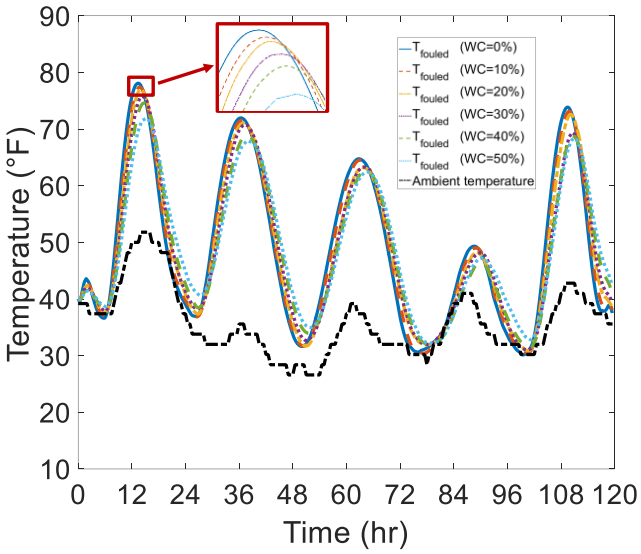

(a)

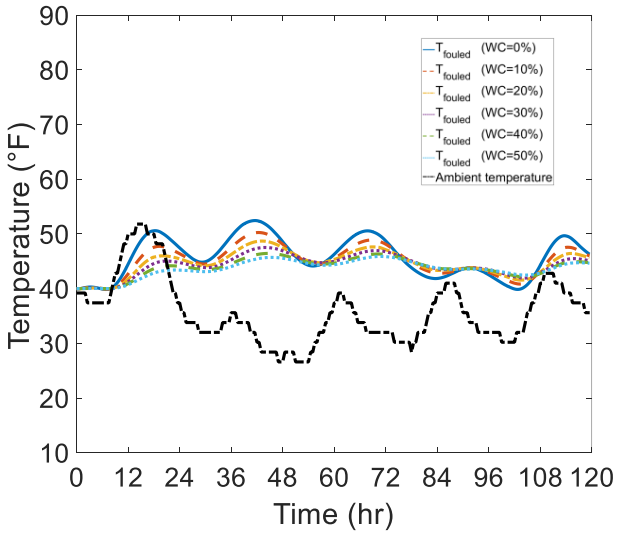

(b)

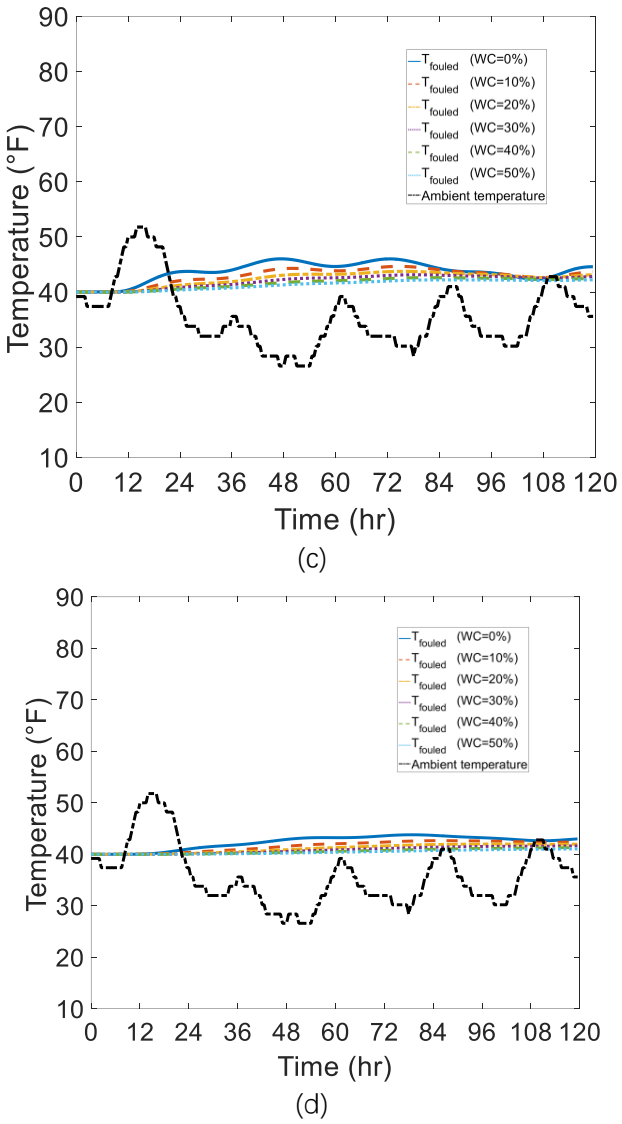

Figure 51. Comparison between ballasts with different amount of water: (a) At the surface layer; (b) At 4-inch deep layer; (c) At 8-inch deep layer; (d) At 12-inch deep layer

The temperature difference between ballast with various amounts of water is also plotted for surface, 4-inch, 8-inch, and 12-inch deep layers, as shown in Figure 52. A similar pattern is observed for ballast at all depths: more water result in a larger temperature difference between ballasts. For example, figure 52a shows the temperature difference on the top surface, it is observed that, for the ballast with no water, the temperature difference is around 5 degrees. After adding water, the temperature difference increases to more than 10 degrees. A similar pattern could be observed in all other layers. The simulation result indicates that water makes a major difference in the thermal behavior of the ballast.

Interestingly, when comparing the temperature difference at a different depth, it is shown that the maximum temperature difference is observed at the top surface, which ranges from 4 to 14 degrees as shown in Figure 53a. For ballast at the 4-inch deep layer, the temperature difference is reduced

to a smaller range of 3 to 8 degrees as shown in figure b. And for ballast at 8-inch and12-inch deep layer, the temperature difference is reduced to a range of fewer than 5 degrees. The result indicates that with the participation of water, the maximum thermal behavior difference should be observed on the top surface. Comparing to the result of case 1, which indicates that the maximum temperature difference should be observed at the 4-inch-deep layer, the participation of water makes it easier to detect the different thermal behavior on the top surface. This finding is important for the application of thermal-based technologies, for that it is convenient and efficient for those technologies to detect the surface temperature.

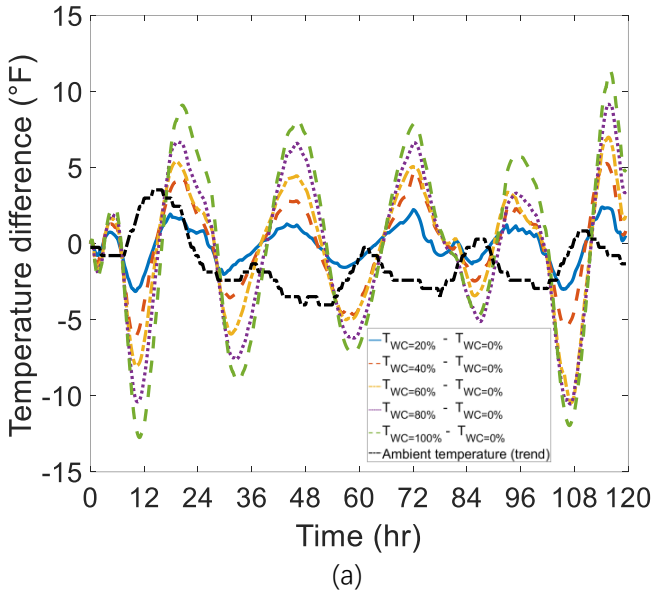

(a)

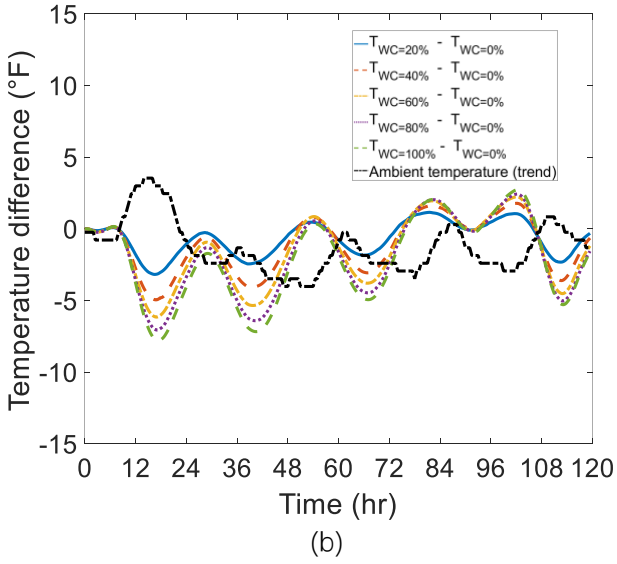

(b)

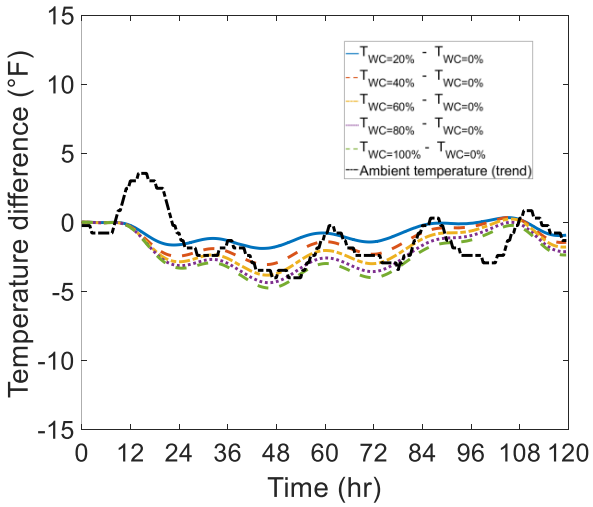

(c)

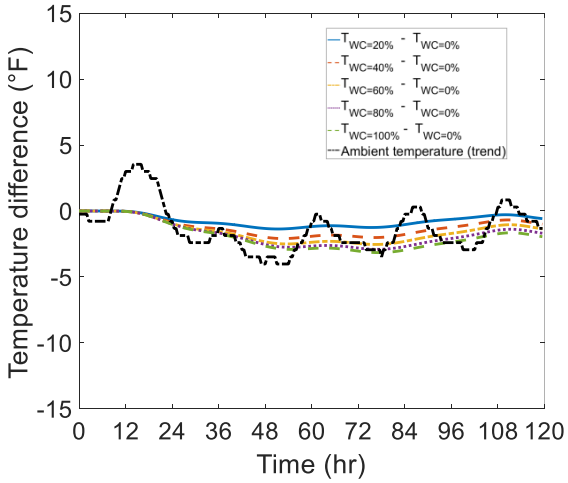

(d)

Figure 52. The temperature difference between ballast with different water content: (a) At the surface layer; (b) At 4-inch deep layer; (c) At 8-inch deep layer; (d) At 12-inch deep layer

SECOND ROUND OF EXPERIMENTS, COMPARING THE MEASUREMENTS FROM THE THERMOCOUPLES WITH THOSE OF THE FLIR CAMERA

Methodology and Test Configuration

This section introduces the overall approach to the second round of tests investigating the applicability of FLIR technology for detecting the early stages of railroad ballast fouling by comparing the readings from the thermocouples and the thermal camera.

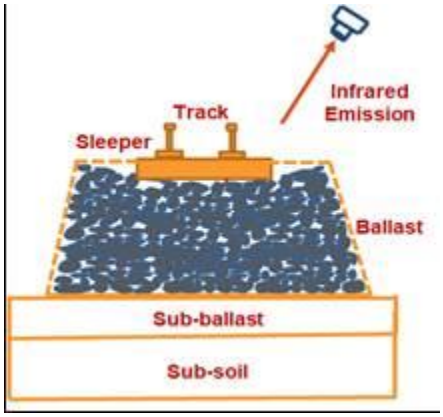

Figure 53 Measuring the temperature of the top surface of ballast by a thermal camera

Figure 54 Fouled, partially fouled, and clean ballast samples

The tests are conducted outdoors and during the summer. Ballast and contaminants used in laboratory tests were obtained from railroad companies to keep the properties and thermal characteristics as close as possible to real-world conditions.

Three 14”×22” ×10” containers are filled with clean, partially fouled, and fouled ballast, and are placed in direct contact with the ground to keep the temperature of the bottom of the containers the same. It should be noted that the contact point of the containers with the ground represents the point where the sub-ballast meets the sub-soil foundation in the real world.

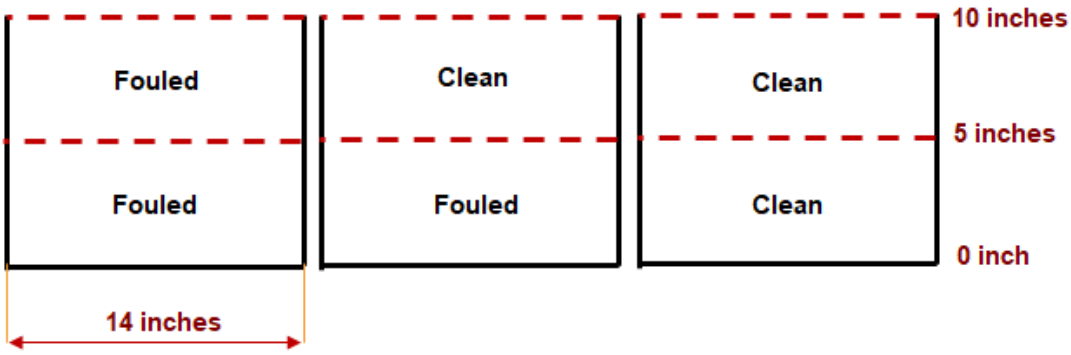

Figure 55 The depths of clean and fouled layers in each container

The fouling ratio of the samples was measured by mass and it was set to be 50% for all tests. The partially fouled container is filled with one layer of fouled ballast at the bottom and one layer of clean ballast on top of it. The depth of the layers was chosen to be the same to simulate the process of fouling started from the bottom and reaching halfway through to the top surface. Fouling progressed up to 50% of the height was assumed to be a reasonable choice since fouling below that level may not affect the top surface temperature to a great extent. On the other hand, fouling above that level may require the maintenance of the completely fouled ballast.

The experiments are divided into two groups: dry ballast measurements, and the measurements involving ballast samples with water content. For the dry-ballast test, the temperature of the top surface of the containers is captured by the thermal camera for time intervals ranging from 14 to 20 hours and during different days. In the second phase, water equivalent to 50% of the weight of the contaminants is added to partially fouled and fouled containers and the experiments are repeated for wet-fouled-ballast under the same conditions.

There are some limitations to utilizing the thermal imaging method. One of these limitations is that it is not capable of measuring the ambient temperature directly. However, based on the research conducted at the University of Edinburgh**Error! Reference source not found.**, the temperature of the rail could be measured as an alternative. This study suggests that the temperature of the rail could be a reasonable replacement for the direct measurement of the ambient temperature due to the low thermal capacity of steel and consequently its fast reaction to the environment. For this reason, a piece of rail was also placed next to the containers since putting it on top of the containers would cast a shadow on the top surface and affect the temperature readings by the thermal camera.

To prevent its direct contact with the ground, a wooden sleeper was placed underneath the rail as shown in 

Figure 54.

FLIR Camera VUE Pro R is utilized for thermal imaging. The camera has an accuracy of +/- 5 Celsius and is mounted on a simple beam structure at 60 inches above the ground and forming a 45-degree angle below the horizon to minimize the adverse effects of high reflection angles. To keep the conditions repeatable, as well as to eliminate the effects of noise that could have been caused by movement, all the tests are conducted in a stationary configuration. The captured thermal images are imported to FLIR Research IR software to get the equivalent temperatures in Fahrenheit. The emissivity and humidity are set to 0.95 and 50% respectively based on the manufacturer's recommendation. Finally, the output of FLIR Research IR software is imported to MATLAB for further analysis.

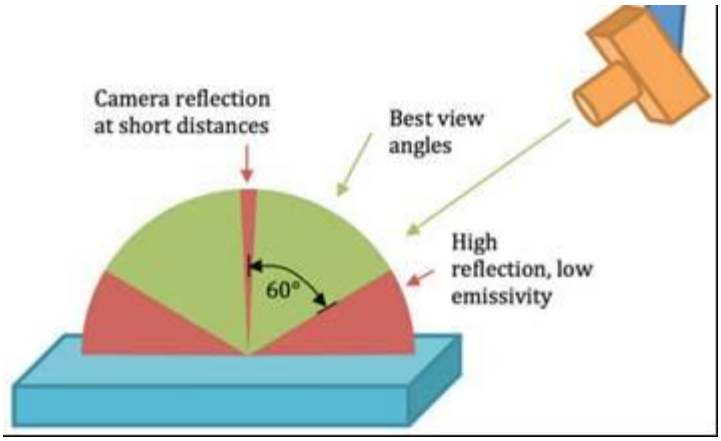

Figure 56 Best view angle to minimize the effects of high reflectivity

Results and Discussion

This section discusses the results of the conducted experiments based on the configuration explained in the previous section. Studying the degree to which the ambient conditions influences the thermal system and measuring the subsequent temperature difference accurately by thermal imaging were the objectives of the designed experiments.

The thermal characteristics of clean and fouled ballast, as well as the effects of water content, were previously studied. Results show that adding contaminants and water to the ballast increases its thermal capacity and causes a difference in the temperature of the different depths during daily heating and cooling cycles. The mentioned research was performed using thermocouples which are reasonably accurate, but the thermal imaging is only limited to the top surface temperature measurements and the extent of this difference was the parameter of interest in the conducted experiments.

The solar radiation could be considered as the main source of thermal energy affecting the system. Being able to measure the ambient temperature changes and possibly maximize these effects to observe the behavior of the system under such extreme conditions was another goal of the experiments. Lastly, limitations and accuracy of measurement by the thermal camera itself were crucial for making conclusions about the applicability of this specific model of FLIR camera and in turn gaining more insight about the possibility of applying this technology in practice.

Test A The first test involved dry ballast samples and was carried out in July with the ambient temperature ranging from 80 to 93 degrees Fahrenheit. This fact was employed to maximize the effects of the solar radiation on the ballast sample, as well as to provide information about the upper bound of the temperature difference between clean, and partially fouled ballast. The experiment started at 9:00 AM and finished at 10:00 PM monitoring the temperature of the top surface of the three ballast containers by capturing thermal camera every 60 seconds.

The temperature readings (in °F) stored in each pixel of the infrared image was obtained from FLIR Research IR software and then imported to MATLAB. The temperature of each ballast container was averaged over the specified area as shown in

Figure 57. The temperature of the shiny and tarnished part of the rail was also measured to investigate whether the rail is a good representative for the ambient temperature changes or not. Each thermal image represents a point in time and by plotting all of these points, the temperature curve for each sample is obtained. The noise of the measurement was filtered by applying a moving average for every 20 points. Figure 58 illustrates the temperature readings for clean, partially fouled, completely fouled, as well as the tarnished part and the shiny part of the rail. Second measurements using handheld thermocouples demonstrated the accuracy of thermal imaging to be within the range specified in device specifications.

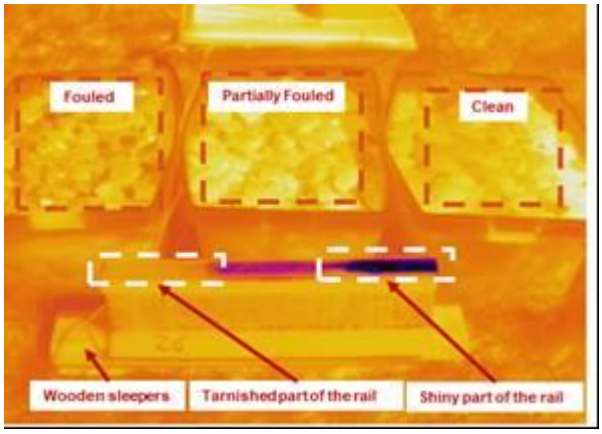

Figure 57 Thermal image of the samples

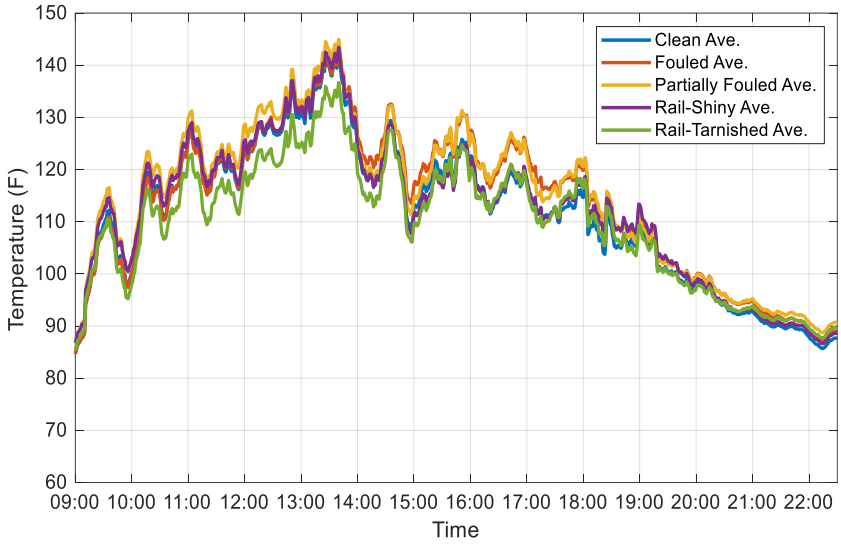

Figure 58 Temperature of dry ballast samples, the tarnished and the shiny parts of the rail during the dry-ballast-test

The overall trend of the curves follows the ambient temperature changes during a typical day but there are low amplitude fluctuations along the curves. Further investigation and closely monitoring the test conditions suggests that these fluctuations are most probably caused by the varying amount of reflected infrared energy emitted from the top surface. This amount could vary during the day for two reasons: the varying projection angle of incoming sun rays, and the uneven surface reflecting the incoming infrared energy.

The relative temperature difference with respect to the tarnished part, as well as to the shiny part of the rail are plotted in
Figure 59. The difference with respect to the tarnished part of the rail ranges from zero to ten degrees Fahrenheit with a maximum of roughly ten degrees at high noon. Fouled ballast sample shows the highest difference before the midday and the partially fouled ballast reaches the same level after 12:00 pm. The clean ballast sample shows a lower temperature difference compared to the other samples throughout the day. However, the difference with respect to the shiny part of the rail follows the opposed pattern before 12:00 pm. In fact, readings indicate that the temperature of the shiny part of the rail was lower than the clean and partially fouled and clean sample even though the thermal capacity of steel is lower than the ballast.

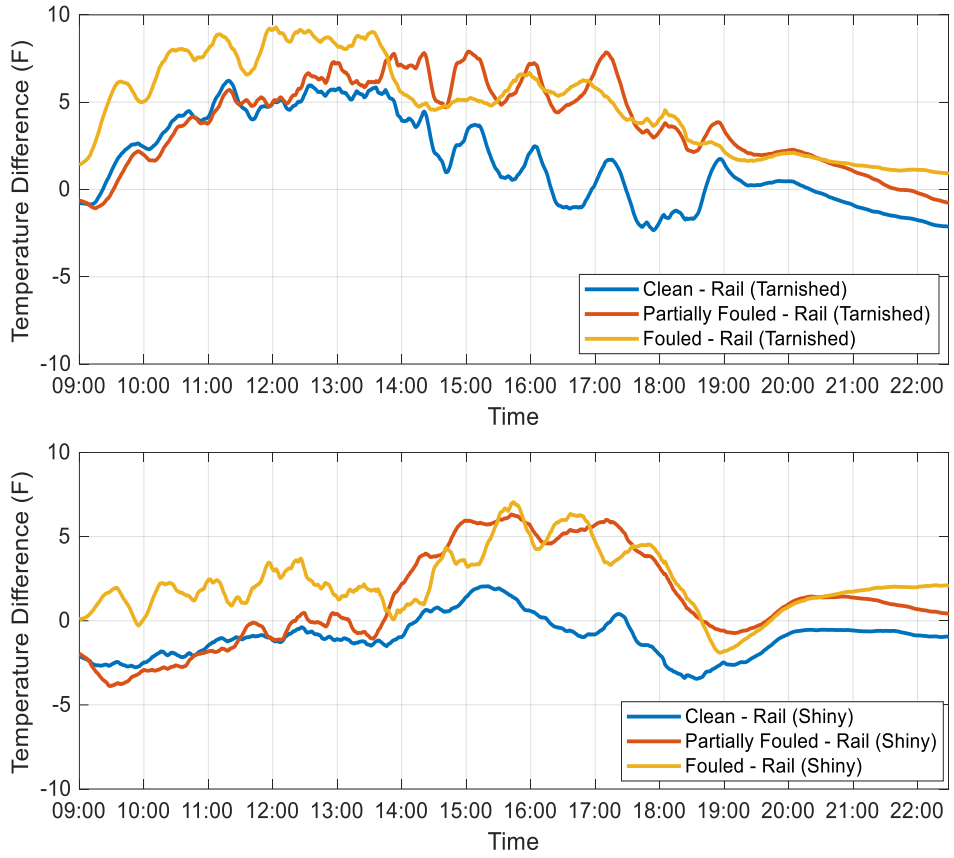

Figure 59 Top: relative temperature difference with respect to the tarnished part of the rail. Bottom: relative temperature difference with respect to the shiny part (dry ballast test)

To further study this discrepancy, the relative temperature difference between the shiny and the tarnished part of the rail was analyzed. As depicted in
Figure 60, the shiny part of the rail shows a higher temperature within a two-hour time interval before and after the high noon, when the angle between the sun rays and the top surface of the samples is close to 90 degrees. This result, in tandem with side experiments involving other materials, suggests that high reflectivity of the surface adversely affects the accuracy of readings

by the thermal camera. A part of the issue originates from the fact that the reflectivity is set for the whole thermal image and couldn't be set selectively for different parts of the thermal image.

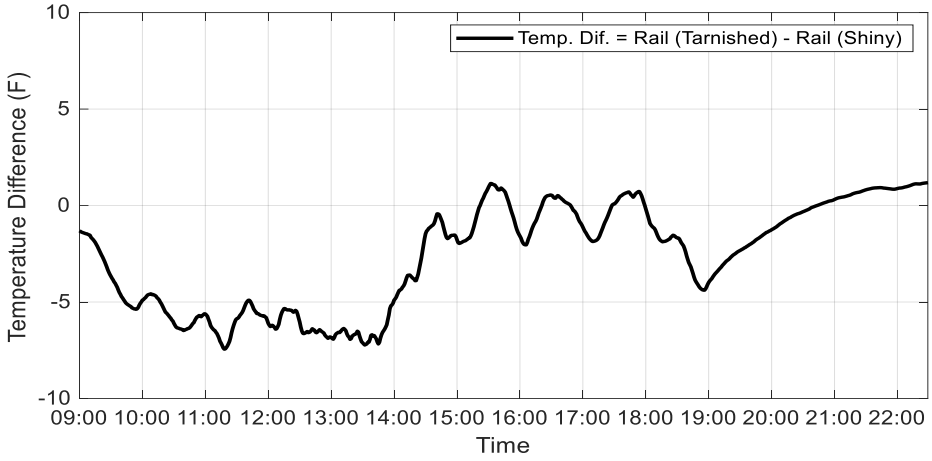

Figure 60 Temperature between the shiny part and the tarnished part of the rail (dry ballast test)

In real-world conditions, oftentimes the thermal imaging systems are set up in an over-head configuration. This in part implies that mostly the shiny part of the rail will be exposed to the thermal camera. Considering the effects of high reflectivity in presence of ambient light, using the temperature of the rail as a representative of the ambient temperature doesn't seem to be a reasonable assumption or to be highly reliable in practice. Needless to say, these conclusions hold for the measurements done using this specific thermal camera model, specified sample sizes and conditions. Even though, thermally there is no certain indicator that the ballast in a specific segment along the railway is fully clean, comparing the range of the temperature difference between the clean and partially fouled/ fouled samples could provide a measure for the possible observable range of difference in practice.

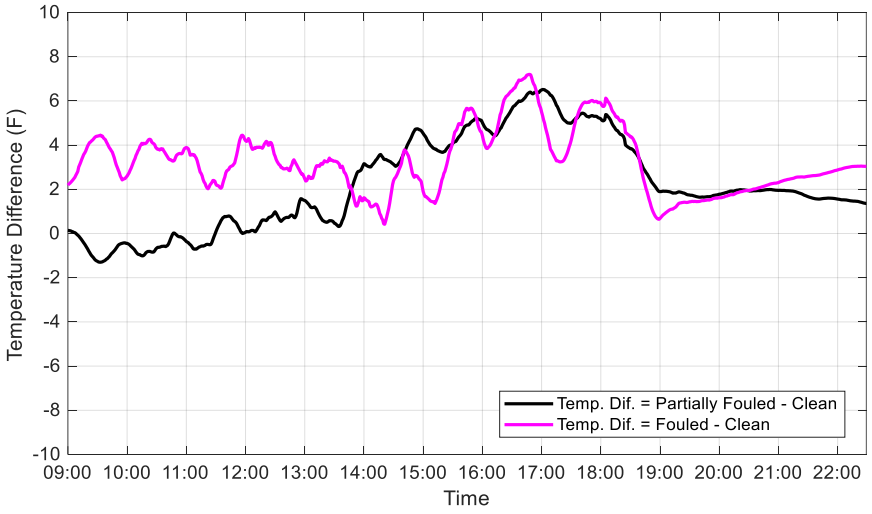

Figure 61 The temperature difference between the clean sample, and dry partially fouled/fouled samples

As shown in
Figure 61, fouled ballast shows a higher temperature than clean ballast throughout the day ranging from 2 to 7 degrees and eventually reaches the same temperature as the clean sample. This physically also makes sense as the fouled ballast has a higher thermal capacity compared to the clean ballast and can retain more thermal energy. The difference gets narrower at high noon since the increased solar radiation heats up the container with lower thermal capacity faster. On the other hand, the partially fouled ballast starts from the same level as the clean ballast and the temperature difference gradually increases as the ambient temperature rises. The lower difference in the morning could be explained by the fact that the top layer of the partially fouled container is made up of clean ballast, but the overall thermal capacity is higher considering the fouled bottom layer.

To observe the pattern of the temperature difference, the changing rate of the temperatures of the ballast containers was also analyzed. Figure 62 shows the relative changing rate of temperature for a one-hour time step. The curves follow the same pattern except for the following time intervals: from 12:30 pm to 14:00 pm, and 17:30 pm to 19:00 pm. The remarkable point is that the latter happens very close to the time interval at which we observe the highest temperature differences in Figure 61. The highest temperature difference and the sharpest rate of temperature change happening at the same time suggest that the measurements are to be done during this time interval to best capture the difference between the thermal behavior of clean and partially fouled ballast. The experiments with the dry ballast sample showed promising results in terms of capturing this difference by the thermal camera. However, the range of temperature difference was quite low and not capable of implementing in practice. A series of experiments with ballast samples containing water were also conducted to measure the highest capturable temperature difference with the thermal camera.

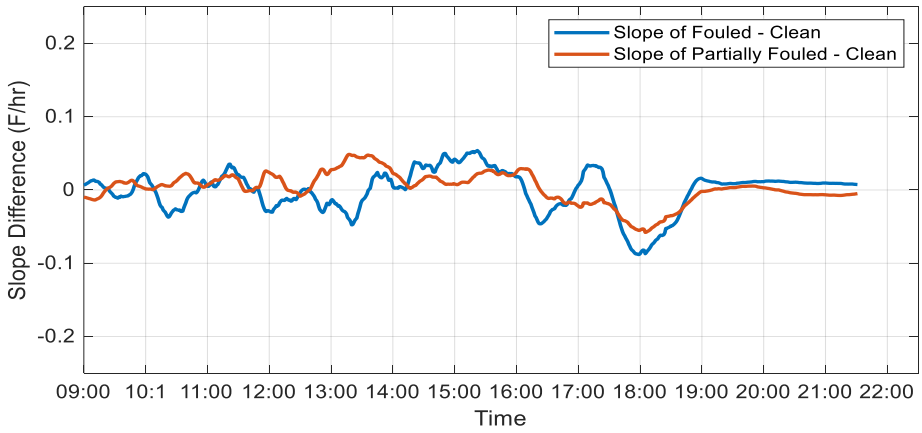

Figure 62 The relative rate of temperature change between dry partially fouled/fouled samples and the clean sample

Test B For the second test, water was added to the partially fouled and fouled ballast samples. The water content was measured by mass and set to be 50% of the weight of the contaminants in the container. The test was performed within a few days from day first test to replicate the

ambient conditions as much as possible. The experiment started at 11:00 AM and finished at midnight. The thermal images were captured at the same rate as the first test, 60 images/hr.

As shown in
Figure 63, adding water caused the ballast samples to behave more differently. The range of temperature difference has reached a maximum of 10 degrees and this difference has become more pronounced when the ballast samples are cooling down. This could be explained by the increased thermal capacity of the ballast samples containing water. The temperature difference between the partially fouled and the clean sample, and between fouled and clean samples are demonstrated in Figure 63. The trend of the difference between fouled and clean samples is very similar to the dry test. The temperature difference is lower in the beginning but remains at that level, slightly sloping down after 19:00. This behavior perfectly matches the physical sense as adding water increases the thermal capacity of the samples containing contaminants. The clean ballast sample cannot retain water and we can observe that its behavior is almost the same as dry test.

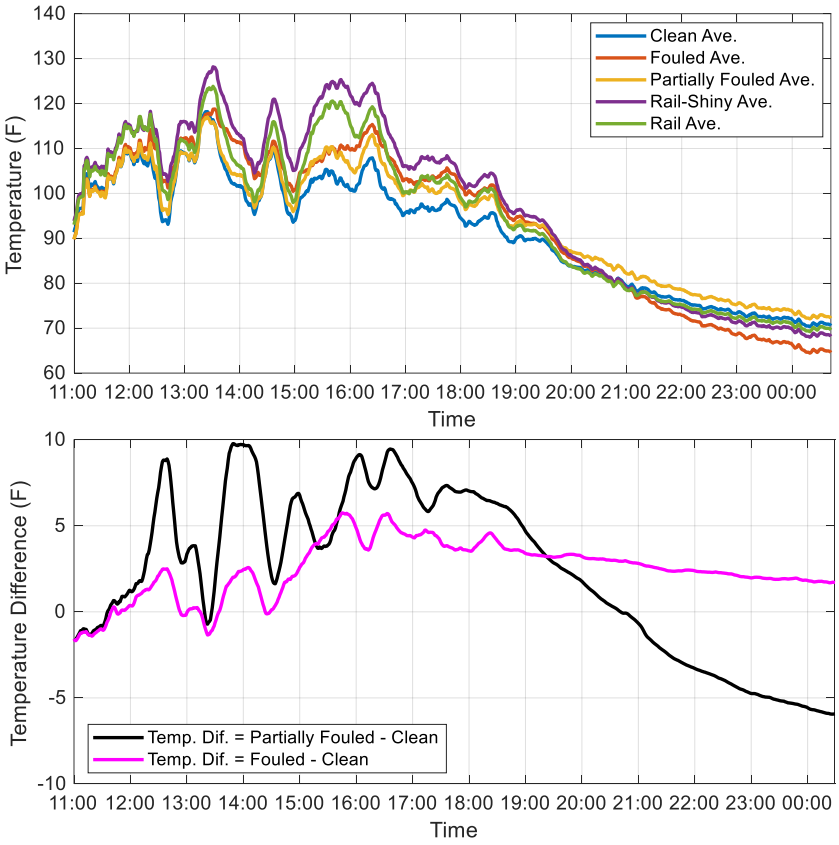

Figure 63 Top: Temperature of wet ballast samples, the tarnished and the shiny parts of the rail. Bottom: The temperature difference between the clean sample, and wet partially fouled/fouled samples

Despite the dry ballast test, the temperature difference between the partially fouled and the clean samples is higher than the difference between the fouled and clean samples with water content. In fact, one expects to observe a higher difference from the latter during the wet ballast test. This

phenomenon could be explained considering the fact that the overall thermal capacity of wet fouled ballast allows it to absorb more thermal energy but react less compared to the partially fouled ballast sample. On the other hand, the top surface of the partially fouled sample shows sharper temperature difference because the wet fouled ballast at the bottom layer of the container increases the temperature at the contact point of the two layers. This, in turn, increases the temperature of the top layer of the partially fouled container which is made up of clean ballast for two reasons: the first one is that the thermal capacity of the clean ballast in lower and the second one is that the temperature at the bottom of this layer is higher. These two combined could explain the higher temperature difference at the top surface of the partially fouled ballast. Although the clean sample has the lowest thermal capacity and is expected to have higher temperature, it shows a lower temperature at the top surface since the convective heat transfer between the ballast and the air (occurring in the voids among the stones) as well as the lower temperature at the contact point with the ground allows it to cool down faster compared to the counterparts.

The relative changing rate of the temperature difference for the wet ballast test is also demonstrated in Figure 64 with a one-hour time step. Similar to the dry ballast test, it could be observed that the highest difference occurs at high noon and there is a shallower difference close to sunset. The difference is that the former is starker, and the latter is smoother for the wet ballast test as opposed to the dry ballast test.
Figure 63 and Figure 64 combined with the results from the dry ballast test suggests that the difference between the thermal behavior of partially fouled/fouled and clean ballast samples is best observable during the peak of heating up and cooling down cycles at high noon and close to sunset.

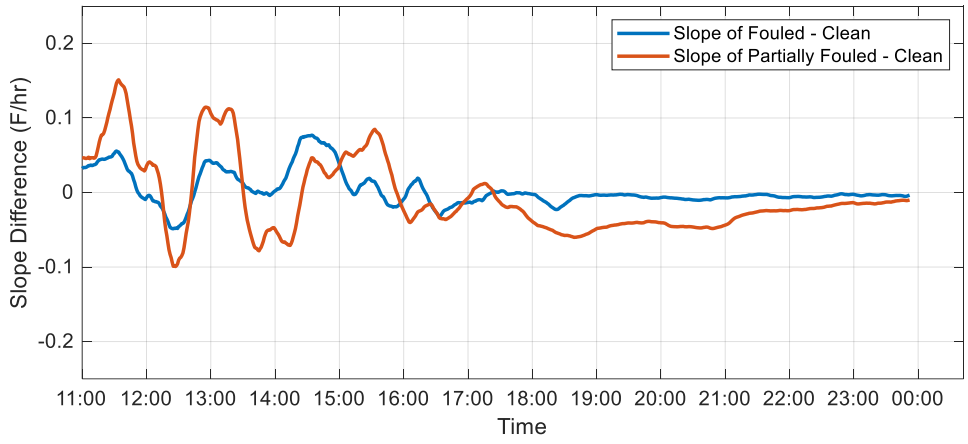

Figure 64 The relative rate of temperature change between wet partially fouled/fouled samples and the clean sample

Both experiments show that there is a difference between the temperature of the partially fouled and clean ballast samples at the top surface. However, the range of temperature difference is very limited, 10 degrees at maximum, and it could easily be disturbed by the noises.

CONCLUSION

The forward-looking infrared radiometer is a novel approach for monitoring and detecting fouled ballast on railway tracks. In this project, efforts are made to verify the effectiveness of the proposed method. The features of the FLIR camera are studied, including the influence of the camera self-heating up, the influence of light, the influence of PPM and the influence of the surface material. The results show that the reading from the camera is relatively stable. Notably, the surface of the material has a major influence on the temperature result, especially for the material with lower emissivity. A series of tests are later performed with the application of FLIR camera in the laboratory and outdoors in both stationary and moving configurations, in order to better understand the effect of fouling on the rate of temperature change of ballast in response to naturally-occurring temperature changes. The test results indicate that fouled ballast heats up slower than clean ballast. The larger the fouling ratio of fouling results is, the slower the rise or drop in ballast temperature would be. Also, the test shows that the FLIR camera is able to show the temperature difference between clean and fouled ballast in both stationary and moving configuration, which indicates the possibility of applying this technology.

The research is further continued with the application of thermocouples. Thermocouples have the advantage of measuring the temperature at deeper layers and at a lower cost than FLIR camera. A series of experiments are conducted to compare the temperature of different depth of ballast under different conditions. Those conditions include dry and wet ballast, fully fouled ballast and partially fouled ballast. The test results show that the only difference is observed between clean and fouled ballast with the participation of water, where a temperature difference of 10 degrees is observed for deeper layers while a temperature difference of 5 degrees is observed for the ballast on the top surface. Although a temperature difference is shown, the test is limited by the small scale compared to the real railroad ballast. For example, the laboratory test cannot simulate the wind flowing through the ballast without causing a large area of shadow. Also, the influence of railway track and sleeper is still unknown. More field tests should be conducted to learn more information on the application of this technology.

This project later explores the thermal behavior of ballast by using numerical and simulation methodology. Theoretically, the thermal characteristics of the clean and fouled ballast are different, which potentially leads to different thermal behavior. One-dimensional conductive heat transfer numerical model is built for ballast under clean and different fouling conditions. The model is validated by an indoor experiment configuration. The tests result agrees with the simulated result quite well. Upon validating these models, a large set of simulation studies are performed to examine the thermal behavior of ballast with different amounts of fouling and water under real temperature and solar irradiance variations in five days, which are collected by National Renewable Energy Laboratory (NREL). The simulation study is conducted under two typical ballast fouling conditions: fouling with and without water. In the case of fouling without water, the temperature at various depths (0-12in) of clean ballast is compared with those with different fouling ratios including 20%, 40%, 60%, 80%, and 100% by volume. For the case of fouling with water, we evaluate the effect of various water contents (10%, 20%, 30%, 40%, and 50% by weight of the contaminant) on the thermal behavior of fouled ballast. The simulation results for the case of fouling without water show that there is a temperature difference between the clean ballast and fouled ballast at the depth ranging from 0 to 12in. Interestingly, it is found that the temperature

difference peaks at the 4-in-deep layer of ballast. The results also indicate that increasing the amount of fouling results in less temperature variation in response to the ambient temperature changes for the ballast at all depths that are considered. For the case of the fouling with water, the results show that adding water into the fouled ballast contributes to a larger temperature difference to the clean ballast at all depths. In addition, the maximum temperature difference is observed at the top surface rather than the depth of 4-in observed in the case of fouling without water. It is because of the participation of the water results in a significant increase in the thermal capacity of the bulk ballast. It is concluded that fouled ballast behaves differently form clean ballast in both top surface and deeper layers under natural-occurring daily ambient temperate changes. However, the test results are limited to the laboratory setup itself. To analyze the thermal behavior of the ballast, a conductive heat transfer model is applied. The results show that a temperature difference of 10 degrees Fahrenheit is observed between clean and fouled ballast, with a fouling ratio of 100% by volume. However, for ballast with less fouling and without water, less temperature difference is observed.

The results from the second round of tests indicate that the reflectivity of the top surface of the rail affects the reading of the thermal camera during the day and limits the possibility of providing a reliable substitute for the direct measurement of the ambient temperature. Water content in ballast samples is observed to increase the range of temperature difference between the top surface of partially fouled/fouled ballast and clean ballast. Comparing the rates of temperature change indicates different behaviors during the heating up and cooling down cycles at high noon and close to sunset. These time intervals are the best candidates for making measurements as the temperature difference reaches the highest level possible. Test results demonstrate a temperature difference of 7-8 degrees between the top surface of wet partially fouled ballast and clean ballast on average. Temperature differences up to 10 degrees were also observed for short periods of time during the wet ballast tests. Despite the positive test results in terms of capturing the temperature differences, this range could easily be disturbed by noises in real-world conditions and requires more accurate measurements and a full accounting of the effects of noises to be applicable in the field.

REFERENCES

1. Lim, W. L., "Mechanics of Railway Ballast Behavior," Ph.D. diss, University of Nottingham, 2004.
2. Indraratna, B., and Salim, W., "Mechanics of Ballasted Rail Tracks: a Geotechnical Perspective," CRC Press, 2005.
3. Janardhanam, R., and Desai, C. S., "Three-dimensional Testing and Modeling of Ballast," Journal of Geotechnical Engineering 109, no. 6 1, pp. 783-796, 1983.
4. Indraratna, B., Ngoc, T. N., and Rujikiatkamjorn, C., "Behavior of Geogrid-reinforced Ballast under Various Levels of Fouling," Geotextiles and Geomembranes 29, no. 3, pp. 313-322, 2011.
5. Anbazhagan, P., Bharatha, T. P., and Amarajeevi, G., "Study of Ballast Fouling in Railway Track Formations," Indian Geotechnical Journal 42, no. 2, pp. 87-99, 2012.
6. Bruzek, R., Stark, T. D., Wilk, S. T., Thompson, H. B., and Sussmann, T. R., "Fouled Ballast Definitions and Parameters," Joint Rail Conference, 2016.
7. Indraratna, B., Tennakoon N. C., Nimbalkar, S. S., and Rujikiatkamjorn, C., "Behaviour of Clay-fouled Ballast under Drained Triaxial Testing," pp. 410, 2013.
8. Jack, R., and P. Jackson., "Imaging Attributes of Railway Track Formation and Ballast using Ground Probing Radar," NDT & E International 32, no. 8, pp. 457-462, 1999.
9. Brough, M., Stirling, A., Ghataora, G., and Madelin, K., "Evaluation of Railway Trackbed and Formation: a Case Study," NDT & E International 36, no. 3, pp. 145-156, 2003.
10. Xu, Q., and Zhang, L., "The Mechanism of a Railway Landslide Caused by Rainfall," Landslides 7, no.2, pp. 149-156, 2010.
11. Leng, Z., and Imad, A., "Railroad Ballast Evaluation using Ground-penetrating Radar: Laboratory Investigation and Field Validation," Transportation Research Record: Journal of the Transportation Research Board 2159, pp. 110-117, 2010.
12. Al-Qadi, I. L., Xie, W., Roberts, R., and Leng, Z., "Data Analysis Techniques for GPR Used for Assessing Railroad Ballast in High Radio-frequency Environment," Journal of transportation engineering 136, no. 4, pp. 392-399, 2010.
13. Shao, W., Bouzerdoum, A., Phung, S. L., Su, L., Indraratna, B., and Rujikiatkamjorn, C., "Automatic Classification of Ground-penetrating-radar Signals for Railway-ballast Assessment," IEEE Transactions on Geoscience and Remote Sensing 49, no. 10, pp. 3961-3972, 2011.
14. Clark, M. R., Gillespie, R., Kemp, T., McCann, D. M., and Forde, M. C., "Electromagnetic Properties of Railway Ballast," NDT & E International 34, no. 5, pp. 305-311, 2001.
15. Silvast, M., Nurmikolu, A., Wiljanen, B., and Levomaki, M., "An Inspection of Railway Ballast Quality using Ground Penetrating Radar in Finland," Proceedings of the Institution of Mechanical Engineers, Part F: Journal of Rail and Rapid Transit 224, no. 5, pp. 345-351, 2010.
16. Hugenschmidt, J., "Railway Track Inspection using GPR," Journal of Applied Geophysics 43, no. 2-4, pp. 147-155, 2000.
17. Bagavathiappan, S., Lahiri, B. B., Saravanan, T., Philip, J., and Jayakumar, T., "Infrared Thermography for Condition Monitoring–A Review," Infrared Physics & Technology 60, pp. 35-55, 2013.
18. Arpaci, V. S., and Arpaci, V. S., "Conduction Heat Transfer," Vol. 237, Reading, MA: Addison-Wesley, 1966.

19. Gallardo-Saavedra, S., Hernández-Callejo, L., and Duque-Perez, O., "Technological Review of the Instrumentation Used in Aerial Thermographic Inspection of Photovoltaic Plants," Renewable and Sustainable Energy Reviews 93, pp. 566-579, 2018.
20. Burud, I., Vukovic, M., Thiis, T., and Gaitani, N., "Urban Surfaces Studied by VIS/NIR Imaging from UAV: Possibilities and Limitations," in Sixth International Conference on Remote Sensing and Geoinformation of the Environment, vol. 10773, pp. 16, 2018.
21. Ariwoola, R. T., "Use of Drone and Infrared Camera for a Campus Building Envelope Study," 2016.
22. Lee, E. Ju., Shin, S. Y., Ko, B. C., and Chang, C., "Early Sinkhole Detection using a Drone-based Thermal Camera and Image Processing," Infrared Physics & Technology 78, pp. 223-232, 2016.
23. Amici, S., Turci, M., Giulietti, F., Giammanco, S., Buongiorno, M. F., Spina, A. L., and Spampinato, L., "Volcanic Environments Monitoring by Drones Mud Volcano Case Study," Int. Arch. Photogramm. Remote Sens. Spat. Inf. Sci, pp. 5-10, 2013.
24. Omar, T, and Nehdi, M. L., "Remote Sensing of Concrete Bridge Decks using Unmanned Aerial Vehicle Infrared Thermography," Automation in Construction 83, pp. 360-371, 2017.
25. Tan, Y., Chen, Y., Peterson, A. W., and Ahmadian, M., "Monitoring and Detecting Fouled Ballast Using Forward-Looking Infrared Radiometer (FLIR) Aerial Technology: Possibilities and Limitations," Joint Rail Conference, 2019.
26. Hosseini, S., Tan, Y., and Ahmadian, M., "Forward-Looking Infrared Radiometry (FLIR) Application for Detecting Ballast Fouling," Joint Rail Conference, 2020.
27. Shen, J., Lassue, S., Zalewski, L., and Huang, D., "Numerical study on the thermal behavior of classical or composite Trombe solar walls," Energy and Buildings, 39.8, pp. 962-974, 2007.
28. Gatmiri, B., and Delage, P., "A formulation of fully coupled thermal-hydraulic–mechanical behavior of saturated porous media—numerical approach," International Journal for Numerical and Analytical Methods in Geomechanics, 21.3, pp. 199-225, 1997.
29. Choi, J. C., Park, J., and Lee, S. R., "Numerical evaluation of the effects of groundwater flow on borehole heat exchanger arrays," Renewable Energy, 52, pp. 230-240, 2013.
30. Wang, J., and Bras, R. L., "Ground heat flux estimated from surface soil temperature," Journal of Hydrology, 216, pp. 214-226, 1999.
31. Andre, S., and Degiovanni, A., "A theoretical study of the transient coupled conduction and radiation heat transfer in glass: phonic diffusivity measurements by the flash technique," International Journal of Heat and Mass Transfer, 38, pp. 3401-3412, 1995.

ACKNOWLEDGEMENTS

The authors wish to thank and acknowledge the US Department of Transportation, University Transportation Center Program (RailTEAM UTC) for funding support for this research.

ABOUT THE AUTHORS

Mehdi Ahmadian, Ph.D., J. Bernard Jones Chair Professor

Dr. Mehdi Ahmadian is a Dan Pletta Professor of Mechanical Engineering at Virginia Tech, where he also holds the position of Director of Center for Vehicle Systems and Safety (CVeSS), and the Railway Technologies Laboratory (RLT). Dr. Ahmadian has authored more than 130 archival journal publications and more than 250 conference publications, including a number of keynote lectures. He has served as Editor or Editor-in-Chief for four journals on Vehicle System Dynamics, Vibration and Control, Shock and Vibration and Automobile Engineering. Dr. Ahmadian is Fellow of American Society of Mechanical Engineers of the American Institute for Aeronautics and Astronautics (AIAA). He has received many distinguished scholar awards.

Yongwen Tan

Dr. Yongwen was a visiting scholar when he worked on this research project. His research interests are machine learning, machinery fault diagnosis, railway ballast condition monitoring. He obtained his Ph.D. from Southwest Jiaotong University of China.

Sayed Mohammad Hosseini

Mr. Sayed Mohammad Hosseini was a graduate research assistant in the Department of Mechanical Engineering. He received his PhD in Civil and Environmental Engineering and his BSc and MS educations in Chemical Engineering. His research interests are colloids and surface sciences as related to synthesis, self-assembly, colloidal stability, and functionalization of nanoparticles.